Journal of Computational Physics **152,** 192–230 (1999)
Article ID jcph.1999.6241, available online at http://www.idealibrary.com on IDEAL®

Assessment of Numerical Accuracy of PDF/Monte Carlo Methods for Turbulent Reacting Flows

J. Xu and S. B. Pope

Sibley School of Mechanical and Aerospace Engineering, Cornell University, Ithaca, New York 14853
E-mail: xujun@mae.cornell.edu

Received July 20, 1998; revised February 3, 1999

This study is to explore the numerical features of a particle-mesh algorithm developed for a stand-alone joint velocity-frequency-composition PDF method for turbulent reactive flows. Numerical experiments are performed on a piloted-jet nonpremixed turbulent flame of methane to characterize and quantify various numerical errors in terms of numerical parameters: number of particles per cell N_{pc}, number of cells M^2, and time step Δt. First, a stationary solution is obtained and is verified to be independent of the time step Δt. Then, the total numerical error is identified as statistical error, bias, and discretization error. It is revealed that the statistical error converges as $N_{pc}^{-1/2}$, and the bias as N_{pc}^{-1}. The statistical error can be reduced by time-averaging or by performing multiple independent simulation (e.g., with a parallelized program). Finally, the scheme is shown to be second-order accurate—the spatial discretization error converging as M^{-2}. A modified turbulence frequency model based on the turbulence production-to-dissipation ratio is shown to improve the numerical behavior of the turbulence model. These results demonstrate that the particle-mesh method is convergent. Also, the optimal numerical parameters, minimizing computational cost subject to a specified error tolerance, are estimated. An error reduction scheme, similar to Richardson extrapolation, is proposed and shown to be quite effective in reducing the deterministic error.

Key Words: PDF/Monte Carlo methods; numerical convergence; turbulent reactive flows.

1. INTRODUCTION

It is of significance in engineering applications to predict complex turbulent reactive flows. The accuracy of such predictions depends mainly on two ingredients: turbulence models and numerical solution algorithms. The purpose of turbulence modeling is to describe the physics of turbulent flows as accurately as possible, with the resulting computation being

0021-9991/99 $30.00

economically feasible. On the other hand, accurate numerical algorithms are required to solve the modelled equations. Both of these factors affect the accuracy of the numerical prediction of turbulent reactive flows. In the context of *probability density function* (PDF) methods, it is noted that less attention has been paid to the accuracy of numerical algorithms.

Traditional turbulence models, including two-equation models [24, 53] and second-moment closures [23], are based on Reynolds averaging techniques, and yield modelled equations for statistical moments. In comparison to these models, PDF methods achieve closure through a modelled transport equation for the one-point, one-time probability density functions of certain fluid properties in a turbulent flow [8, 36]. The advantage of PDF methods is that both convection and reaction are represented exactly without modelling assumption. Also, a tremendous amount of statistical information contained in the PDFs obviously provides a fuller description of turbulent flows than two-equation models or second-moment closures. During the past decade, the progress in PDF methods has been made from several aspects: adopting a more advanced joint velocity-frequency-composition PDF method which provides a model for the turbulent time scale [50]; introducing modelling techniques developed in second-moment closures [13, 39, 50]; and developing a computationally efficient scheme to treat detailed reaction chemistry [42]. These models have been successfully applied in modeling several inert flows [6, 30], reactive flows, and turbulent flames [1, 16, 29, 32, 46].

Different numerical solution algorithms are required for turbulence models of different levels. Moment closures result in a set of partial differential equations. These equations are usually solved numerically by finite difference or finite volume methods [17]. In contrast to moment-closure model equations, the modelled PDF transport equation has a completely different structure. From early times in the development of PDF methods, Monte Carlo techniques have been employed in which the PDF is represented by an ensemble of particles [35]. Stochastic differential equations (SDEs), which are usually in the form of Langevin equations, are then constructed to model the particle properties, e.g., velocity and compositions, such that the particles exhibit the same PDF as turbulent flows.

Monte Carlo methods are widely used in computational physics [19] to solve high-dimensional problems such as PDFs. Their application in PDF methods has processed through different stages. In the first method developed, the particles were located at grid nodes in physical space [35]. Pope [36] then suggested that it is preferable to use the method in which the particles are continuously distributed. Later, a hybrid method was implemented in the code *PDF2DS* in which composition PDFs were calculated by Monte Carlo methods while a finite-volume method was applied to solve for the mean velocity, dissipation, and mean pressure fields [3, 5, 18, 32]. More recently, a stand-alone particle-mesh algorithm was developed for the joint velocity-frequency-composition model [40]. A similar method was implemented in the code *PDF2DV*. This is a code to calculate statistically stationary two-dimensional (plane or axi-symmetric) turbulent reactive flows using the joint velocity-frequency-composition PDF method. It has been applied in several published calculations [1, 10, 46, 50].

The purpose of this work is to study the numerical accuracy of the particle-mesh algorithm for PDF methods, in particular the *PDF2DV* code. In *PDF2DV*, the joint velocity-frequency-composition PDF transport equation is solved by a Monte Carlo particle-mesh method. The flow domain is divided into a total number M^2 of cells (uniform or non-uniform) while the fluid is represented by a number of stochastic particles N. The modelled SDEs for particle

properties are solved by a pseudo-time marching scheme with time step Δt. Therefore, the numerical parameters in a *PDF2DV* calculation consist of M^2, Δt, and N, or the number of particles per cell N_{pc} ($N_{pc} \equiv N/M^2$). These parameters essentially determine the accuracy of numerical solutions.

Usually, weak convergence, i.e., the convergence of expectations or moments, instead of the PDF itself is sought for PDF methods. The numerical convergence of PDF/Monte Carlo methods is largely determined by the numerical solution to the modelled SDEs and the estimation of mean fields from stochastic particles. Numerical solutions to stochastic differential equations have been well studied [26, 21]. Also, it has been proved that ensemble averages computed from Langevin equations converge to the correct values if the ensemble averages become time independent [25]. However, the Langevin equations of particle evolution in PDF methods are essentially different from the standard form in that the mean fields are part of coefficients in the SDEs and need to be approximated by their corresponding ensemble averages. Such a feedback of the ensemble averages into the Langevin equations introduces new sources of numerical error [40, 55]. In previous studies, four different types of numerical errors have been identified by considering estimating a mean quantity: statistical error, bias, spatial discretization error, and temporal discretization error [31, 40, 52, 55]. The convergence of numerical solutions requires that these errors vanish as the number of particles per cell N_{pc} and the total number of cells M^2 tend to infinity, and as the time step Δt tends to zero.

One concern with the bias revealed in a previous study is that a model of turbulence frequency based on the square of velocity-strain rate causes the bias to increase when reducing the cell-size [55]. A modified turbulence frequency model is therefore proposed to remove the cell-size dependence of bias.

Using a piloted-jet nonpremixed turbulent flame of methane [27] as a test case, comprehensive calculations are performed to investigate systematically the convergence behavior of the PDF method. Precisely, the numerical errors in *PDF2DV* are characterized and quantified in terms of the numerical parameters. The piloted-jet nonpremixed turbulent methane flame provides a good test case for this study since it has relatively simple boundary conditions, and a comprehensive experimental data set is available [28]. This flow has been selected as one of the standard flows for model verification by the International Workshop on Measurement and Computations of Turbulent Nonpremixed Flames [2] and has also been studied by different researchers using PDF methods [4, 18, 29, 33, 46]. Since the focus of this study is on the numerical issues, simple turbulence models and combustion models are used in the calculations to minimize the computational cost, and the comparison of numerical results with experimental data is not emphasized.

In the next section, the joint velocity-frequency-composition PDF model is briefly introduced and the effect of specific modeling assumptions on numerical errors is discussed for the frequency model. Section 3 gives a description of the Monte Carlo particle-mesh method for PDF methods, i.e., the *PDF2DV* code, followed by a discussion of numerical errors. The test case of the piloted-jet nonpremixed methane flame is described in Section 4, where the comparison of numerical solutions with the experimental data by Masri *et al.* [27] is also presented. In Section 5, the detailed convergence behavior is studied by varying numerical parameters. Computational cost subject to a specified error level is estimated in Section 6, and an effective error reduction scheme similar to Richardson extrapolation is described in Section 7. Conclusions are drawn in the final section.

2. JOINT PDF FORMULATION

In this section, the joint velocity-frequency-composition PDF model is described for modeling turbulent reactive flows. The model considered here is similar to that used in several recent studies [1, 10, 46, 52]. The model equations are given here for completeness and to make precise the variant of the model being used.

For a turbulent reactive flow, we define the mass density function (mdf) $\mathcal{F}$ and the one-point, one-time Eulerian mass-weighted joint PDF (JPDF) $\tilde{f}$ of velocity $\mathbf{U}(\mathbf{x}, t)$, composition vector $\phi(\mathbf{x}, t)$, and turbulence frequency $\omega(\mathbf{x}, t)$ by

$$\begin{aligned}\langle\rho\rangle\,\tilde{f}(\mathbf{V}, \psi, \theta; \mathbf{x}, t) &= \mathcal{F}(\mathbf{V}, \psi, \theta; \mathbf{x}, t)\\ &\equiv \rho(\psi)\langle\delta(\mathbf{U}-\mathbf{V})\delta(\phi-\psi)\delta(\omega-\theta)\rangle,\end{aligned} \tag{1}$$

where $\langle\ \rangle$ denotes a mean quantity, ρ is the density as a function of compositions, and $\mathbf{V}$, ψ, and θ are the sample spaces for $\mathbf{U}$, ϕ, and ω, respectively. A model equation for $\mathcal{F}$ can be devised with the modelling theories developed for turbulent flows [36]. In such a modelled equation, convection and reaction terms are in closed form while models are needed for the pressure-strain-rate correlation, mixing, and dissipation.

The Monte Carlo method is the basic tool to solve the joint PDF equation. Taking a Lagrangian viewpoint, the flow is represented by a set of particles. Stochastic differential equations are then derived to model the evolution of particle properties (e.g., particle velocity) so that a stochastically equivalent system is established: particles exhibit the same JPDF as that given by the PDF transport equation.

Models for particle velocity, turbulence frequency, scalar mixing, and reaction are described in the following subsections. It is worth emphasizing that the models used do not necessarily capture the physics most correctly for the test case considered, but are chosen mostly for the purpose of minimizing the computational work.

2.1. *Velocity Model*

In PDF methods, the fluid particle velocity $\mathbf{U}^+(t)$ is modelled by the stochastic particle velocity $\mathbf{U}^*(t)$. Langevin models have been developed at different levels for $\mathbf{U}^*(t)$ [13, 39, 50]. Since, in this study, there are many computations for different numerical parameters, to minimize the computational cost, the simplified Langevin model (SLM) is chosen

$$d\mathbf{U}^*(t) = -\frac{\nabla\langle p\rangle}{\langle\rho\rangle}\,dt - \left(\frac{1}{2}+\frac{3}{4}C_0\right)\Omega(\mathbf{U}^*(t)-\tilde{\mathbf{U}})\,dt + (C_0 k\Omega)^{1/2}\,d\mathbf{W}, \tag{2}$$

where $\tilde{}$ denotes a density-weighted mean quantity, for example, $\tilde{\mathbf{U}} \equiv \frac{\langle\rho\mathbf{U}\rangle}{\langle\rho\rangle}$, p is pressure, $\mathbf{W}(t)$ is an isotropic Wiener process, Ω is the conditional mean turbulence frequency (defined below), k is the turbulence kinetic energy (defined by $k = \widetilde{u_i u_i}/2$, where $\mathbf{u} = \mathbf{U} - \tilde{\mathbf{U}}$), and C_0 is a model constant (Table I). SLM is equivalent to the Rotta model at the second-moment-closure level [39].

Given the particle velocity $\mathbf{U}^*(t)$, the particle position $\mathbf{X}^*(t)$ evolves by

$$d\mathbf{X}^*(t) = \mathbf{U}^*(t)\,dt. \tag{3}$$

TABLE I
Model Constants

C_0	$C_{\omega 1}$	$C_{\omega 2}$	C_3	C_4	C_ϕ	C_Ω
2.1	0.56	0.9	1.0	0.25	2.0	0.6893

2.2. *Stochastic Model for Turbulence Frequency*

A length or time scale is also needed in PDF methods. Several different approaches have been used in previous applications. In the early development [15], the time scale was assumed to be uniform across free shear flows. As in other turbulence models, however, to remedy this deficiency, one can use the mean dissipation (e.g., the $k-\epsilon$ model [24]) or the turbulence frequency equation (e.g., the $k-\omega$ model [53]) as information on the time scale. Such efforts have led to the joint velocity-dissipation-composition model [43] or the joint velocity-frequency-composition PDF model [50]. The advantages of the latter are discussed by Van Slooten *et al.* [50]. Here, the stochastic turbulence frequency model in [50] is modified and used in the subsequent calculations.

The stochastic model for particle frequency $\omega^*(t)$ is

$$d\omega^*(t) = -C_3(\omega^* - \tilde{\omega})\Omega\, dt - S_\omega \Omega \omega^*(t)\, dt + [2C_3C_4\tilde{\omega}\Omega\omega^*(t)]^{1/2}\, dW, \tag{4}$$

where W is an independent Wiener process. The model details, such as the definition and interpretation of ω^* and the conditional turbulence frequency Ω, are given in [50]. However, this model is slightly different in that the mean frequency is replaced by the conditional mean frequency in the second term on the right-hand side to keep the consistency of definition: the dissipation of energy $\tilde{\epsilon} = k\Omega$. Note that the specification of the coefficients in Eq. (4) guarantees that ω^* is non-negative, and the numerical implementation of the model ensures that this property is preserved.

In Eq. (4), S_ω is the source of turbulence frequency. In previous applications, this term is modeled as [6, 50]

$$S_\omega = C_2 - C_1 \frac{S_{ij}S_{ij}}{\tilde{\omega}^2}, \tag{5}$$

where S_{ij} is the mean rate of strain tensor,

$$S_{ij} = \frac{1}{2}\left(\frac{\partial \tilde{U}_i}{\partial x_j} + \frac{\partial \tilde{U}_j}{\partial x_i}\right), \tag{6}$$

and the constants C_2 and C_1 are assigned the values 0.9 and 0.08, respectively. Although Eq. (5) offers some advantages by relaxing the linkage between the energy and dissipation (or frequency) [11], and gives reasonable results, it is found that this form of S_ω causes numerical problems: it is one of the major sources of bias in the particle-mesh method for PDF models; it also causes the bias to increase with grid refinement. The reason is that, in the particle-mesh method, mean velocities are essentially estimated by ensemble means over particles. Thus, the estimated mean velocities carry fluctuations (of order $N_{pc}^{-1/2}$). As shown by Xu and Pope [55], the estimation of $S_{ij}S_{ij}$ generates relative large bias and causes

the bias to increase when the mesh size is decreased. To circumvent this numerical difficulty, a modified model for S_ω is suggested to replace (5), namely

$$S_\omega = C_{\omega 2} - C_{\omega 1}\frac{P}{\tilde{\epsilon}} = C_{\omega 2} - C_{\omega 1}\frac{P}{k\Omega}, \tag{7}$$

where P is turbulence production

$$P = -\widetilde{u_i u_j}\frac{\partial \tilde{U}_i}{\partial x_j}, \tag{8}$$

and model constants $C_{\omega 1}$ and $C_{\omega 2}$ are specified in Table I.

Obviously, by specifying the production in the form used in the standard $k-\epsilon$ model [53], Eq. (7) reduces to Eq. (5). However, with the use of Eq. (7), the quite small correlation between the estimated Reynolds stress $\widetilde{u_i u_j}$ and the estimated mean velocity is found not to produce significant bias and to be able to remove or weaken the mesh dependence of bias. This is an example of the establishment of turbulence models being influenced by its impact on the numerical implementation.

2.3. *Mixing Model*

The Lagrangian approach is also used to model the scalar properties following a particle $\phi^+(t)$. That is, $\phi^+(t)$ is modelled by a stochastic process $\phi^*(t)$. The effects of molecular diffusion are accounted for by a mixing model. Again, for the sake of saving the amount of computational time, the simplest model—IEM or LMSE model [7]—is applied

$$d\phi^*(t) = -\frac{1}{2}C_\phi \Omega(\phi^*(t) - \tilde{\phi})\,dt, \tag{9}$$

where the standard model constant C_ϕ is used (Table I). Mixing models are crucial in the PDF calculations of turbulent nonpremixed flames with finite-rate kinetics, and it is well established that the IEM model is problematic in this respect [48]. However, reasonable results are obtained when it is used in conjunction with equilibrium or flamelet models—as here.

2.4. *Flamelet Model*

To reduce computational work, instead of more advanced models such as reduced chemistry [47] and ISAT [42], a flamelet model is adopted for the treatment of chemical reaction. The flamelet model is a good choice for this study because of its minimal computational cost and reasonable accuracy for the flame conditions encountered in this study. The flamelet model views a turbulent flame as an ensemble of laminar flamelets. The structure of flamelets is then represented by a function of prescribed parameters (namely mixture fraction ξ and scalar dissipation χ) and is available in the form of a flamelet library. The mixture fraction in the test case of this study (see Section 4) is defined by

$$\xi = \frac{Z_i - Z_{i2}}{Z_{i1} - Z_{i2}}, \tag{10}$$

where the subscripts 1 and 2 refer to fuel and oxidant, respectively, and Z_i is the mass fraction of element i. Therefore, in the jet ξ is unity while it is zero in the coflow.

The flamelet library for methane–air combustion is provided by Peters' group [34]. It is further simplified in this study. That is, instead of defining a scalar field as a function of both ξ and χ, we use a library with a constant χ (namely, $\chi = 2.5\ \mathrm{s}^{-1}$) but variable ξ. This simplification reduces the flamelet model to be a lookup table in ξ. Therefore, all other scalar fields, in particular the density $\rho(\xi)$, are inferred from ξ. Since the only independent scalar field is ξ, Eq. (9) reduces to

$$d\xi^*(t) = -\frac{1}{2} C_\phi \Omega (\xi^*(t) - \tilde{\xi})\, dt. \tag{11}$$

No doubt this economical description of the thermochemistry is an over-simplification, and indeed it is observed to cause some discrepancies in the calculations presented below. But there is no reason to suppose that this has an impact on the numerical issues studied here. More realistic and accurate treatments of the thermochemistry are described by, for example, Saxena and Pope [46].

2.5. *Modelled PDF Equation*

With the above models, the density-weighted JPDF of velocity, frequency, and mixture fraction is

$$\mathcal{F}(\mathbf{V}, \psi, \theta; \mathbf{x}, t) = \langle \rho \rangle\, \tilde{f}(\mathbf{V}, \psi, \theta; \mathbf{x}, t) \equiv \rho(\xi) \langle \delta(\mathbf{U} - \mathbf{V}) \delta(\xi - \psi) \delta(\omega - \theta) \rangle, \tag{12}$$

where ψ is the sample variable of ξ. Then, one-point statistics of the flow can be computed from $\tilde{f}$ or $\mathcal{F}$. For example, the density-weighted mean $\tilde{Q}$ of a property Q is expressed as

$$\begin{aligned} \tilde{Q} = \frac{\langle \rho Q \rangle}{\langle \rho \rangle} &= \int_{-\infty}^{\infty} \int_{-\infty}^{\infty} \int_0^{\infty} \int_0^1 Q^*(\mathbf{V}, \psi, \theta)\, \tilde{f}(\mathbf{V}, \psi, \theta)\, d\psi\, d\theta\, d\mathbf{V}, \\ &= \frac{1}{\langle \rho \rangle} \int_{-\infty}^{\infty} \int_{-\infty}^{\infty} \int_0^{\infty} \int_0^1 Q^*(\mathbf{V}, \psi, \theta) \mathcal{F}(\mathbf{V}, \psi, \theta)\, d\psi\, d\theta\, d\mathbf{V}. \end{aligned} \tag{13}$$

The transport equation for $\tilde{f}(\mathbf{V}, \psi, \theta; \mathbf{x}, t)$ can be derived following the standard procedures [36] from the SDEs (2), (4), and (11)

$$\begin{aligned} \frac{\partial \tilde{f}}{\partial t} = &-V_i \frac{\partial \tilde{f}}{\partial x_i} + \frac{1}{\langle \rho \rangle} \frac{\partial \langle p \rangle}{\partial x_i} \frac{\partial \tilde{f}}{\partial V_i} + \left(\frac{1}{2} + \frac{3}{4} C_0 \right) \Omega \frac{\partial}{\partial V_i} [\tilde{f}(V_i - \tilde{U}_i)] \\ &+ \frac{1}{2} C_0 k \Omega \frac{\partial^2 \tilde{f}}{\partial V_i \partial V_i} + \Omega \frac{\partial}{\partial \theta} (\tilde{f} \theta S_\omega) + C_3 \Omega \frac{\partial}{\partial \theta} [\tilde{f}(\theta - \tilde{\omega})] \\ &+ C_3 C_4 \Omega \tilde{\omega} \frac{\partial^2}{\partial \theta^2} (\tilde{f} \theta) + \frac{1}{2} C_\phi \Omega \frac{\partial}{\partial \psi} [\tilde{f}(\psi - \tilde{\xi})], \end{aligned} \tag{14}$$

where all model constants are tabulated in Table I.

The PDF transport equation (14) and the SDEs (2), (4), and (11) (in addition to $\tilde{f}$ and the independent variables) involve means obtained from $\tilde{f}$, namely, $\langle \rho \rangle$, $\tilde{\mathbf{U}}$, Ω, k, $\tilde{\xi}$, and $\tilde{\omega}$. Also, the mean pressure $\langle p \rangle$ is to be determined implicitly by mean mass conservation [36]. The estimation of these mean fields as well as other numerical issues is discussed in the next section.

3. NUMERICAL ASPECTS

The Monte Carlo technique has been proved to be a very effective tool to solve the modelled JPDF evolution equation, Eq. (14). The numerical scheme used here is a particle-mesh method in which the joint PDF is represented by an ensemble of particles. The particle properties are evolved by a set of SDEs (e.g., Eq. (2)), and the mean fields (e.g., the mean velocities) are estimated at each grid node. This method is implemented in the code *PDF2DV* and has been applied in several calculations, such as swirling flows [1], compressible flows [6], near wall turbulent flows [10], and flames [46].

In a particle method, the basic numerical ingredients are an integration scheme to advance the particle properties in time; a method of representing and of estimating mean fields; and an algorithm to determine the mean pressure field and to enforce the mean continuity equation (for flows with complex reactions, an efficient algorithm to treat the effects of reaction, such as *ISAT*, is also needed). Although a complete description of the particle-mesh method used here has not been published, these ingredients have been described individually elsewhere. This section presents a general description of the *PDF2DV* code with brief discussions about different numerical ingredients. It also discusses the nature and origin of the numerical errors that are the focus of this study.

3.1. *Particle-Mesh Method and PDF2DV Code*

Using the particle-mesh method, the *PDF2DV* code is designed to model statistically stationary two-dimensional (plane or axi-symmetric) turbulent flows, in particular reactive flows. For any flow considered, the code adopts a rectangular computational domain. The domain is then decomposed into a number of small uniform or non-uniform rectangular cells for the purpose of representing and estimating mean fields. Supposing that there exist M_x cells in the x direction (axial direction for the axi-symmetric case) and M_y cells in the y direction (radial direction for the axi-symmetric case), then the total number of cells is $M^2 = M_x \times M_y$. Denoting the extent of the domain as $\mathcal{L}_x$ in the x direction and $\mathcal{L}_y$ in the y direction, respectively, the cell size is then approximately represented by $h_x = \mathcal{L}_x/M_x$ (x direction) and $h_y = \mathcal{L}_y/M_y$ (y direction). Also, a representative cell size is taken to be $h = \sqrt{\mathcal{L}_x\mathcal{L}_y}/M$. Thus, for a specific flow, M^{-1} is a good non-dimensional measure of the cell size.

The JPDF is represented by an ensemble of N stochastic particles which model fluid particles. Suppose at time t, the nth particle has position $\mathbf{X}^{(n)}$, velocity $\mathbf{U}^{(n)}$, turbulence frequency $\omega^{(n)}$, and mixture fraction $\xi^{(n)}$. All these properties depend only on time t and evolve according to the modelled SDEs (2), (3), (4), and (11), respectively. Therefore, the discrete Lagrangian mdf $\mathcal{F}_N$ is defined as

$$\mathcal{F}_N(\mathbf{V}, \psi, \theta, \mathbf{x}; t) = \Delta m \sum_{n=1}^{N} \delta\big(\mathbf{U}^{(n)} - \mathbf{V}\big)\delta\big(\xi^{(n)} - \psi\big)\delta\big(\omega^{(n)} - \theta\big)\delta\big(\mathbf{X}^{(n)} - \mathbf{x}\big), \quad (15)$$

where Δm is the mass of particles. For the particle system to be a valid representation of the flow, the correspondence

$$\tilde{f} = \langle \mathcal{F}_N \rangle / q \quad (16)$$

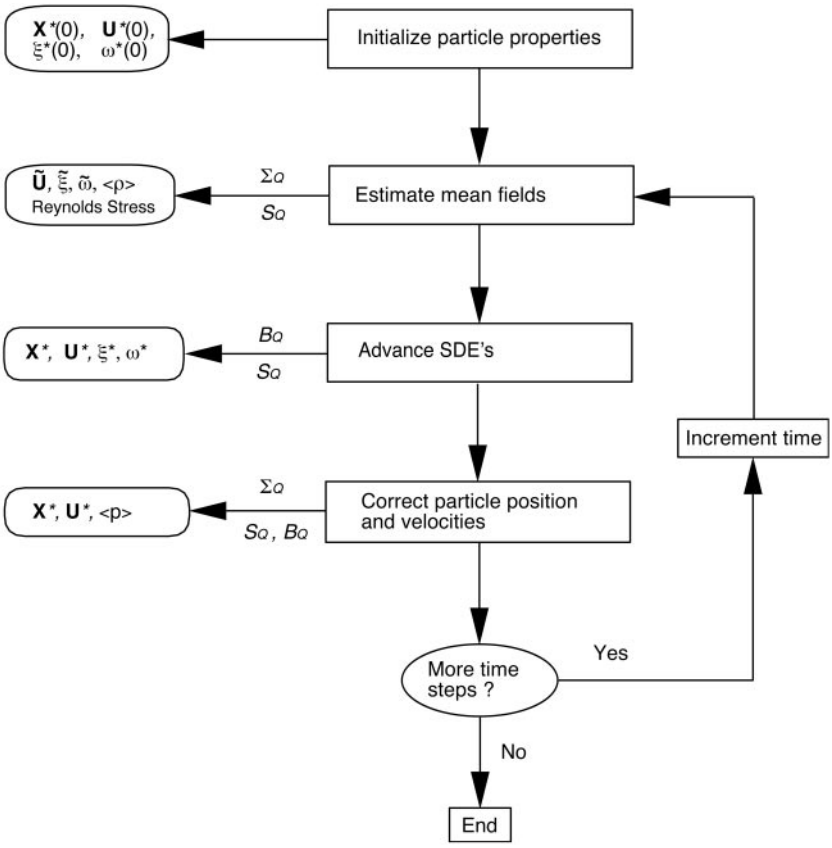

FIG. 1. Diagram of the solution of *PDF2DV*.

is required, where q is the particle mass-density

$$q \equiv \Delta m \sum_{n=1}^{N} \left\langle \delta\left(\mathbf{X}^{(n)} - \mathbf{x}\right) \right\rangle. \tag{17}$$

This matter has been well discussed in Ref. [38].

The solution procedure in a *PDF2DV* calculation is shown in Fig. 1. The particles are initialized for given initial conditions by uniformly distributing them in the physical space and assigning other properties according to appropriate distributions (e.g., joint normal distribution for velocities, gamma distribution for turbulence frequency). Then, a pseudo-time marching scheme [14, 40] is used to solve the SDEs in a discrete form until a statistically stationary state is reached. By this scheme, particle properties advance in a time step Δt (uniform or non-uniform) that is determined by an extended CFL condition

$$\max\left[\Delta t\tilde{\omega}, \min\left(\frac{\tilde{U}\Delta t}{h_x}, \frac{\tilde{V}\Delta t}{h_y}\right)\right] < 1. \tag{18}$$

For an engineering problem, it is desired to obtain the statistics of the flow. Also, at any time t, the mean fields are required to advance the SDEs. Therefore, it is a very important task to calculate or estimate the mean fields. In contrast to the hybrid PDF/Monte

Carlo method (e.g., *PDF2DS* [5]) in which major statistics except for the scalar fields are obtained by solving Reynolds-averaged equations, the estimation of mean fields in *PDF2DV* is accomplished by a nonparametric method—kernel estimation method [12, 51]. In particular, it adopts a cloud-in-cell method in which the mean fields on each grid node are approximated by weighted ensemble means of the particles in the four cells surrounding the node. The mean fields are then represented as linear splines based on the nodal values, so that the mean properties at particle locations are interpolated from the means at the nodes. The details of this method can be found in [9].

Correction algorithms are devised for particle position and velocities to enforce the mean continuity equation and to obtain the mean pressure field. At first, the position correction is performed to satisfy the consistency condition. The consistency condition states that the volume associated with a sub-ensemble of particles equals the geometric volume occupied by the particles. Then, the particle velocities are corrected so that the divergence of the mean mass flux is zero. As a result of the correction, mean pressure is obtained as well. These algorithms have been described in detail in [6, 41]. Finally, note that with the use of the flamelet model, the particle density is deduced from the particle mixture fraction, and the mean density is estimated from particles. All the estimated mean fields are substituted in the SDEs for the next step calculation.

To summarize, in contrast to the hybrid PDF/Monte Carlo method, *PDF2DV* does not need to be incorporated with another CFD code based on moment closure methods, and thus forms a *stand-alone* approach for modeling turbulent reactive flows.

3.2. *Numerical Errors*

With the use of the particle-mesh method, *PDF2DV* solves the SDEs (2), (4), and (11) in discrete forms. The numerical parameters consist of the characteristic cell size h (or total number of cells in the domain M^2), the total number of particles N (or the number of particles per cell N_{pc}), and the time step Δt. Due to finite values of these parameters, the discretization gives rise to various numerical errors.

Convergence of numerical solutions to a stochastic differential system can be interpreted in either a strong or weak sense [26, 21]. Since statistics of the flow are essentially more interesting than modelled particle properties in a PDF/Monte Carlo calculation of engineering problems, the weak convergence is sought for the particle-mesh algorithm. Precisely, this requires that the discrete Lagrangian mdf $\mathcal{F}_N$ represented by N particles should converge in distribution to the actual modelled mdf [38], and consequently any mean quantity evaluated by Eq. (13) should converge to the actual mean. Thus, in the sense of weak convergence, numerical errors in the particle-mesh method are identified as statistical error, bias, and discretization error. The sum of bias and discretization error yields the total deterministic error. Because of the presence of statistical error, the total numerical error in the estimate of a mean field (e.g., mean velocity) is random. Hence, the weak convergence of mean fields should be interpreted in a mean-square sense.

Consider estimating a mean quantity $\langle Q \rangle$ at a fixed position and time in a *PDF2DV* calculation with N_{pc} particles per cell, M^2 total cells in the domain, and time step Δt. Denoting the estimator of $\langle Q \rangle$ as $\{Q\}_{N_{pc},M,\Delta t}$, the total numerical error can be decomposed as

$$\varepsilon_Q \equiv \{Q\}_{N_{pc},M,\Delta t} - \langle Q \rangle = \Sigma_Q + D_Q = \Sigma_Q + B_Q + S_Q, \tag{19}$$

where Σ_Q is the statistical error and D_Q is the deterministic error which is further decomposed into the bias B_Q and the discretization error S_Q.The possible circumstances in which the numerical errors arise in the solution of *PDF2DV* are sketched in Fig. 1. These numerical errors are discussed individually as follows.

First of all, the statistical error Σ_Q is due to the fact that the number of particles representing the joint PDF is finite. As mentioned in the forgoing section, the mean fields in the particle-mesh method are estimated by a cloud-in-cell method. To illustrate the nature of statistical error, consider a simple ensemble mean

$$\{Q\}_N = \frac{1}{N}\sum_{n=1}^{N} Q\big(\mathbf{U}^{(n)}, \xi^{(n)}, \theta^{(n)}\big), \tag{20}$$

where $\mathbf{U}^{(n)}$, $\xi^{(n)}$, and $\theta^{(n)}$ are the properties of the nth particle. For independent and identically distributed particles, a basic result from statistics is that $\{Q\}_N$ is an unbiased estimator of $\langle Q\rangle$. However, for finite N, $\{Q\}_N$ is a random variable, and carries statistical fluctuations—statistical error. The size of the statistical error is measured by the rms statistical error in $\{Q\}_N$, which tends to zero as $N^{-1/2}$ (assuming that the variance of Q exists) according to the central limit theorem [22]. Similarly, the statistical error Σ_Q in the estimator $\{Q\}_{N_{pc},M,\Delta t}$ can be identified as

$$\Sigma_Q = \{Q\}_{N_{pc},M,\Delta t} - \big\langle \{Q\}_{N_{pc},M,\Delta t}\big\rangle. \tag{21}$$

It is expected that Σ_Q converges at the rate of $N_{pc}^{-1/2}$, because the kernel estimates are based on the total number of N_{pc} samples. This behavior of the statistical error has been observed in other PDF/Monte Carlo simulations [31, 40, 52]. Therefore, Σ_Q may be expressed as

$$\Sigma_Q = cN_{pc}^{-1/2}\vartheta, \tag{22}$$

where ϑ is a standardized random variable (with zero mean and unity variance), and c is an error coefficient to be estimated.

Second, bias is a deterministic error resulting from the statistical error. Numerical solutions to Eqs. (2) and (4) are essentially different from the following well-studied standard problem [26]: given coefficients $A(x,t)$ and $B(x,t)$, an initial condition $Z(0)=z_0$, and a stopping time $\mathcal{T}>0$, integrate the stochastic differential equation

$$dZ(t) = A(Z(t),t)\,dt + B(Z(t),t)\,dW(t). \tag{23}$$

The difference lies in the fact that in Eqs. (2) and (4) the coefficients depend also on means of functions of the process, such as $\tilde{\mathbf{U}}$ and $\tilde{\omega}$, which are approximated by ensemble means that contain statistical errors. Xu and Pope [54] use a simplified model to analyze the impact of the feedback of statistical errors in SDE like Eq. (2). They found that such a feedback unfortunately breaks down the independence of the particles, and thus induces bias. In *PDF2DV*, the bias in $\{Q\}_{N_{pc},M,\Delta t}$ is identified as

$$B_Q = \big\langle \{Q\}_{N_{pc},M,\Delta t}\big\rangle - \{Q\}_{\infty,M,\Delta t}, \tag{24}$$

where $\{Q\}_{\infty,M,\Delta t} \equiv \lim_{N_{pc}\to\infty}\{Q\}_{N_{pc},M,\Delta t}$. It is revealed that the statistical errors affecting the drift term in Eq. (2) are the major source of bias [55]. Also, both theoretical analysis

[40, 54] and numerical experiments have shown that the bias scales as the reciprocal of the number of particles

$$B_Q = \frac{b}{N_{pc}}, \tag{25}$$

where b is another error coefficient. This implies that B_Q converges faster than Σ_Q.

Finally, the identification of the discretization error is

$$S_Q = \{Q\}_{\infty, M, \Delta t} - \langle Q \rangle. \tag{26}$$

It consists of two parts: temporal error and spatial error. The finite time step Δt results in temporal error. The pseudo-time marching scheme in *PDF2DV* is second-order accurate, and the temporal error is not a dominant error [14, 40]. Since it has been well studied in [40], the temporal error will not be discussed further in this study. For this reason, hereafter, S_Q mainly contains spatial error. However, there have been very few studies conducted on this error. It can only be studied in inhomogeneous turbulent flows, and thus costs significant computational time. This study takes a great deal to characterize the spatial error.

To summarize, the total numerical error in a *PDF2DV* calculation is composed of statistical error, bias, and discretization error. The definition of these errors are given by Eqs. (21), (24), and (26), and the sum of these equations shows that they form a decomposition of the total error, i.e.,

$$\varepsilon_Q = \Sigma_Q + B_Q + S_Q. \tag{27}$$

Note that the identification presented here is not unique, but it indeed provides a good insight about the nature and origin of numerical errors. Section 5 is devoted to studying the features of these numerical errors.

4. MODEL PROBLEM

The model problem studied is a nonpremixed piloted-jet methane flame described in [28]. An axi-symmetric jet of methane fuel with radius $R_j = 3.6$ mm is centered in an annular pilot ($R_p = 9.0$ mm). The pilot burns a mixture of stoichiometric composition and provides a heat source to stabilize the main jet at the exit plane. The flame is accompanied by an unconfined coflowing stream of air. The bulk velocity in the jet U_J is specified to be $U_J = 41.0$ m/s, the pilot has a velocity $U_P = 24.0$ m/s, and the coflow velocity U_C is 15.0 m/s. These conditions correspond to the L flame in Masri and Bilger [27]. Measurements have been performed for temperatures by thermocouple method, velocity by LDA, and compositions by sample probes. Experimental data are provided by Masri *et al.* [28].

The L flame is a good test case for this study. First of all, as experiment indicates, the flame is blue up to $60R_j$ and there is little local extinction. Therefore, a simple chemistry treatment (such as the flamelet model) can be used. Consequently, the usage of the IEM mixing model is also satisfactory. These two models are the simplest models that one can choose and cost the least computational work. Moreover, there have been several PDF calculations of this flame [4, 18, 29, 46]. These computational results also favor the suitability of the models used here.

A cylindrical coordinate system is adopted with x representing the axial direction and y the radial direction. The origin of the coordinate is placed at the center of the fuel jet. The computational domain is taken to be rectangular and divided into a total of M^2 non-uniform rectangular cells. The outflow boundary is far down-stream at $80R_j$ to prevent outlet boundary conditions from influencing the solutions at the locations where experimental data are provided (up to $50R_j$). In the y direction, the outer boundary is at $15R_j$ to cover a sufficiently large uniform region in the coflow. Lengths are normalized by the jet radius $R_j = 3.6$ mm. Hence, the computational domain has the normalized scale: $\mathcal{L}_x = 80$ and $\mathcal{L}_x = 15$. The characteristic velocity is taken to be the coflow velocity $U_C = 15$ m/s which is used to normalize all other velocities. Consequently, frequency is normalized by U_C/R_j.

Initial and boundary conditions are inferred from the experimental data in the similar manner to Masri and Pope [29] and Norris and Pope [33]. In a PDF/Monte Carlo calculation, the initial and boundary conditions are specified for the joint PDF, and specifically defined for particles. At the inlet, the velocity PDF is prescribed to be joint normal, and the appropriate Gamma distribution is assigned to turbulence frequency. Both of them have the prescribed mean derived as follows. The mean velocity and normal Reynolds stresses $\widetilde{uu}$ and $\widetilde{vv}$ are given by experimental data (assuming that $\widetilde{ww} = \widetilde{vv}$). However, the covariance $\widetilde{uv}$ and mean frequency $\tilde{\omega}$ are not measured. It should be noted that for the modified turbulence frequency model based on the production-to-dissipation ratio (Eq. (7)), the boundary conditions for the mean frequency and $\widetilde{uv}$ are more crucial than they are in the original model based on the square of velocity-strain rate (Eq. (5)). The latter is solely dependent on mean rate of strain which is determined by the mean velocity profile alone, while the modified model is affected by both the boundary conditions of $\widetilde{uv}$ and $\tilde{\omega}$ (Eq. (7)). Hence, proper specifications of these conditions are of significance. Here, the covariance $\widetilde{uv}$ is evaluated by

$$\widetilde{uv} = \rho_{uv}(\widetilde{u^2}\widetilde{v^2})^{1/2}, \tag{28}$$

where the correlation coefficient ρ_{uv} is taken to be 0.4 as suggested by Tennekes and Lumley [49] except for the coflow where $\rho_{uv} = 0$. Then, using the equilibrium assumption that production equals dissipation, the mean frequency can be determined by

$$\tilde{\omega} = \frac{P}{k} = -\frac{\widetilde{uv}}{k}\frac{\partial \tilde{U}}{\partial y}, \tag{29}$$

where everything on the right-hand side is known. Boundary conditions other than the inlet conditions include the outflow condition at the outlet boundary and reflecting conditions for the centerline and upper boundaries. These conditions are imposed straightforwardly at the particle level. Finally, particles are initialized so as to have the same conditions as the inlet boundary.

Although the agreement between the experimental data and computational results is not emphasized in this study, such comparisons for mean velocity $\tilde{U}$, mean mixture fraction $\tilde{\xi}$, mean temperature $\tilde{T}$, and mean mass fractions $\tilde{Y}_{CO}$ are shown in Fig. 2. In comparison to the previous computations [4, 29, 46], these results are reasonable for the purpose of this study considering the simple models being used. The difference in the mean temperature is due to the use of the simple flamelet model for thermochemistry.

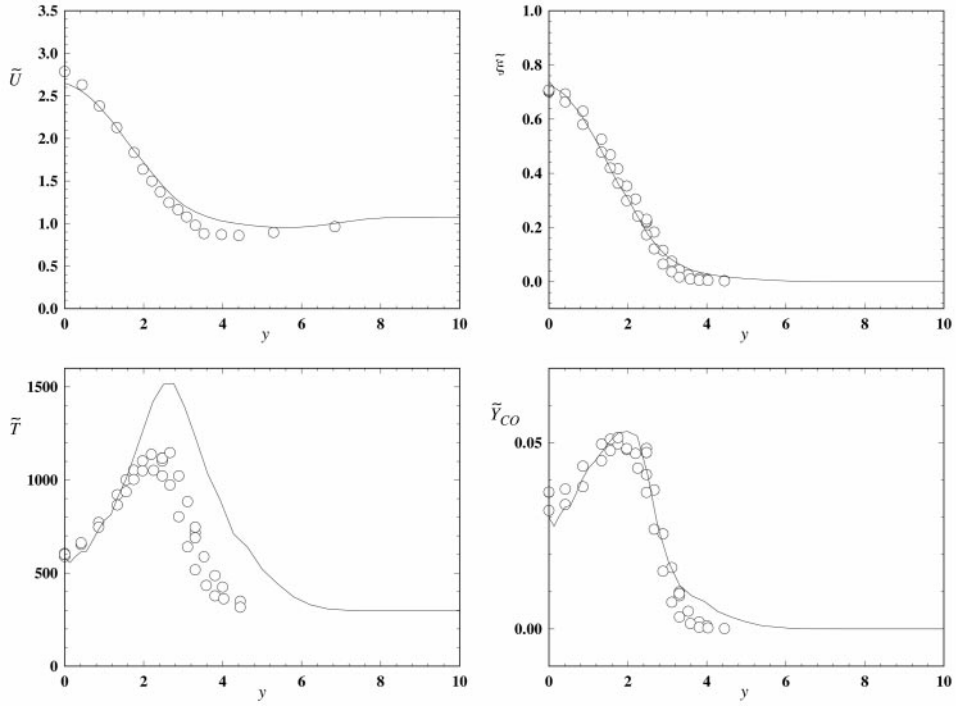

FIG. 2. Comparison of mean profiles at $x = 40$. Solid line, PDF calculation with 40×40 cells, $\Delta t = 0.08$, and $N_{pc} = 200$; symbols, experimental data of Masri *et al.*

5. CONVERGENCE RESULTS

The particle-mesh method implemented in *PDF2DV* involves several numerical techniques, such as nonparametric regression and the numerical solution to stochastic differential equations. For such a complicated algorithm, a complete theoretical analysis of its convergence is unlikely to be possible. Alternatively, this task can be fulfilled by numerical experiments in which by varying numerical parameters, a set of calculations are conducted to isolate different numerical errors so as to characterize and quantify them in terms of different numerical parameters. In this section, using *PDF2DV*, comprehensive calculations are carried out on the piloted-jet flame. The numerical errors identified in Subsection 3.2, i.e., statistical error, bias, and discretization error, are investigated individually by systematically varying the numerical parameters: the number of particles in each cell N_{pc}, the total number of cells M^2, and the time step Δt.

The stationarity of numerical solutions is first inspected. Then, the results about the statistical error are reported followed by a discussion on methods to reduce this error. Bias is investigated, and especially the behavior of the modified turbulence frequency model is explored. Then, an effort is devoted to exploring the behavior of discretization error. Finally, a summary is given.

5.1. *Stationary Solution*

PDF2DV is designed to treat statistically stationary flows, such as the piloted-jet flame. It is therefore expected that the numerical solution reaches a statistically stationary state

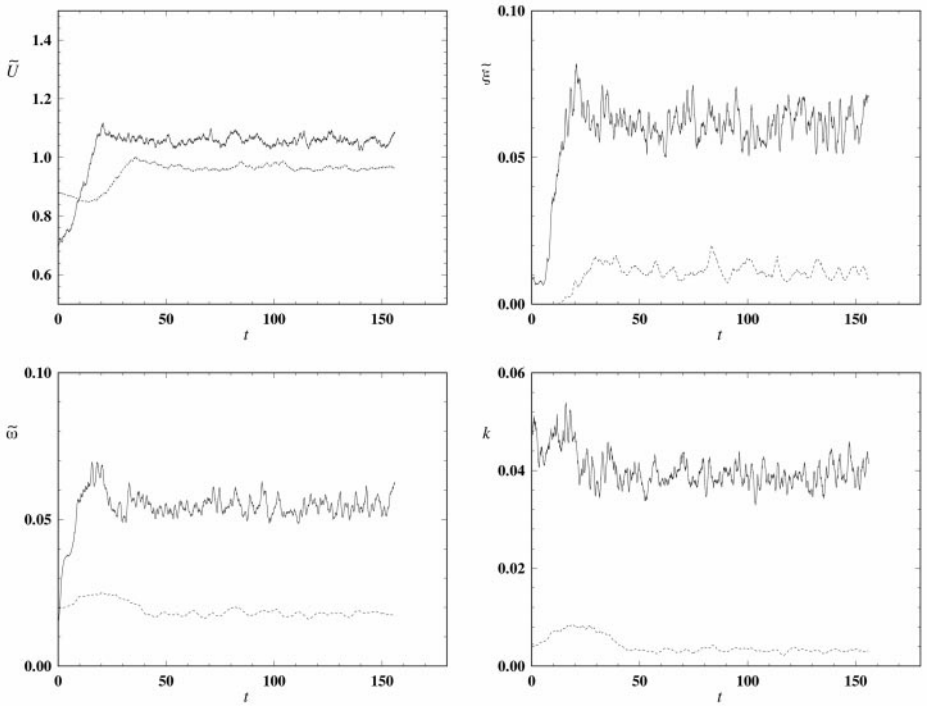

FIG. 3. Stationary solutions. Time series of mean quantities at locations (20, 2.5) (solid line) and (40, 5) (dashed line). Cells, 40×40, $N_{pc} = 200$.

in a finite number of steps N_s in the sense that mean quantities do not evolve with time after $T_s = N_s \Delta t$. Usually, the time to reach stationarity T_s is between 2 and 5 times the flow residence time. Stationarity of the solution is monitored by observing the evolution of mean fields at selected grid nodes. The time series of the means of velocity, frequency, turbulence kinetic, and mixture fraction at two observation locations are shown in Fig. 3. As pointed out in Subsection 3.2, because of using the finite number of particles, the estimated mean quantities embody fluctuations—statistical error. In spite of this, it can be seen that the solutions attain a stationary state around $T_s = 60$, which corresponds to $N_s = 1000$ for $\Delta t = 0.06$.

Although the temporal discretization error due to the time step Δt is not studied in detail here, it is still worth clarifying the concern whether the time step Δt has an impact on the stationary solutions. For this sake, calculations with four different time steps (Table II), but the same cell size and value of N_{pc}, are made. The corresponding profiles of time-averaged

TABLE II
Effects of Time Steps on Stationarity

Δt	Courant number	$\max(\tilde{\omega}\Delta t)$
0.05	0.2344	0.0294
0.06	0.2811	0.0354
0.07	0.3288	0.0412
0.08	0.3751	0.0472

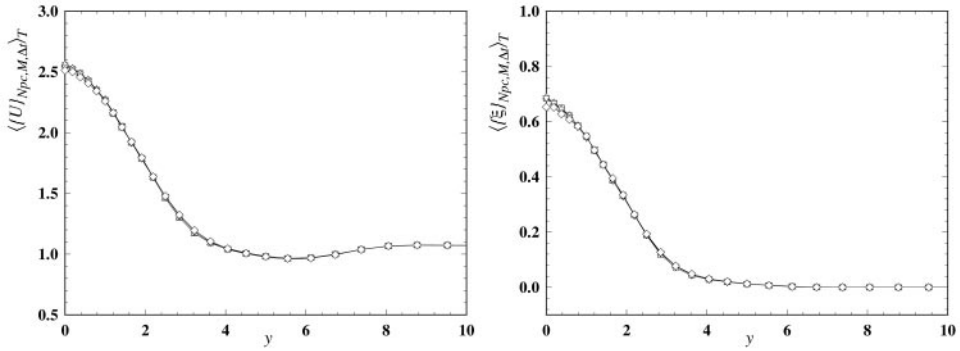

FIG. 4. Profiles of time-averaged mean velocity and mixture fraction at $x = 40$. Symbols, $\square$, $\Delta t = 0.05$; $\triangle$, $\Delta t = 0.06$; $\triangledown$, $\Delta t = 0.07$; $\diamond$, $\Delta t = 0.08$. Cells, 30×30, $N_{pc} = 200$.

mean velocity and mixture fraction (defined in Subsection 5.2) are compared in Fig. 4. Apparently, the difference among the time steps, $\Delta t = 0.05$, 0.06, and 0.07, is negligible.

5.2. *Statistical Error*

Statistical error results from the finite number of particles in each cell. As discussed in Subsection 3.2, for any variable Q, the statistical error is identified as

$$\Sigma_Q = \{Q\}_{N_{pc},M,\Delta t} - \big\langle \{Q\}_{N_{pc},M,\Delta t} \big\rangle. \tag{30}$$

If N_{pc} is infinite, Σ_Q vanishes while it increases as N_{pc} decreases. Σ_Q is usually measured by its standard error

$$\Sigma_Q = N_{pc}^{-1/2} \sigma_Q \vartheta, \tag{31}$$

where ϑ is a standardized random variable and σ_Q is the standard error defined by

$$\sigma_Q^2 = N_{pc} \operatorname{var}\big(\{Q\}_{N_{pc},M,\Delta t}\big). \tag{32}$$

Asymptotically, as N_{pc} tends to infinity, σ_Q becomes independent of N_{pc} so that Σ_Q converges as $N_{pc}^{-1/2}$. Note also that σ_Q is the estimator of the error coefficient c in Eq. (22).

The estimation of σ_Q requires a number of samples of $\{Q\}_{N_{pc},M,\Delta t}$. The ergodic assumption is used for this purpose: that is, instead of sampling from different independent trials, samples are taken from a time series of $\{Q\}_{N_{pc},M,\Delta t}$ during the stationary state. The rms of Σ_Q is estimated by a standard technique (for the same M and Δt) [20], and then plotted against N_{pc} in Fig. 5. The slopes of the least-square straight line fits to the data are close to $-1/2$, thus confirming the expected behavior

$$\Sigma_Q = c_Q N_{pc}^{-1/2} \vartheta, \tag{33}$$

where $c_Q = \sigma_Q$.

Overall, achieving a statistical error level of 5% for $\tilde{U}$ and $\tilde{\xi}$ requires about 400 particles in each cell. However, the statistical error can be reduced through a time-averaging technique. Suppose an additional N_t steps are computed after the solution reaches its stationary state.

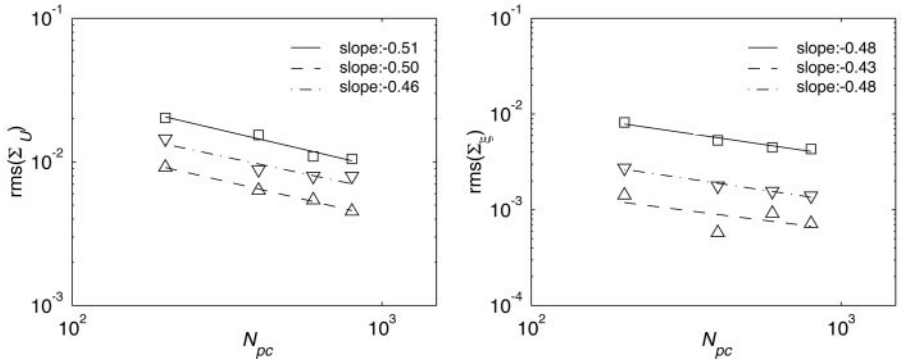

FIG. 5. Statistical error in mean velocity and mixture fraction. □, point (40, 2.5); △, point (40, 5); ▽, point (60, 5). Cells, 30×30. The lines are the least-squares fits to the data.

Then, a statistically stationary time series of $\{Q\}_{N_{pc},M,\Delta t}$ of length $T_t = N_t \Delta t$ is obtained. Generally, such a time series contains a time scale τ, and values on successive time steps are correlated. A time-averaged mean for $\{Q\}_{N_{pc},M,\Delta t}$ is defined by

$$\left\langle \{Q\}_{N_{pc},M,\Delta t} \right\rangle_{T_t} \equiv \frac{1}{T_t} \int_{T_s}^{T_s+T_t} \{Q\}_{N_{pc},M,\Delta t}(s)\, ds. \tag{34}$$

The variance of $\langle \{Q\}_{N_{pc},M,\Delta t} \rangle_{T_t}$ is much less than that of $\{Q\}_{N_{pc},M,\Delta t}$ for large T_t. Therefore, a reduction factor of the statistical error can be defined

$$\mathcal{R}_Q(T_t) \equiv \left[\frac{\mathrm{var}\left(\left\langle \{Q\}_{N_{pc},M,\Delta t} \right\rangle_{T_t} \right)}{\mathrm{var}\left(\{Q\}_{N_{pc},M,\Delta t} \right)} \right]^{1/2}. \tag{35}$$

Note that $\langle \{Q\}_{N_{pc},M,\Delta t} \rangle_{T_t=0} = \{Q\}_{N_{pc},M,\Delta t}$. A standard result of time series analysis [45] shows that

$$\mathcal{R}_Q^2(T_t) = \frac{2}{T_t} \int_0^{T_t} \left(1 - \frac{|s|}{T_t} \right) \rho(s)\, ds, \tag{36}$$

where $\rho(s)$ is the autocorrelation function of the time series. For a large T_t, $\mathcal{R}_Q$ behaves asymptotically as

$$\mathcal{R}_Q \sim \sqrt{\frac{2\tau}{T_t}}, \tag{37}$$

where the time-scale τ is defined by

$$\tau \equiv \int_0^{\infty} \rho(s)\, ds. \tag{38}$$

That is, the time-averaging (over a long time) reduces the statistical error by a factor of $\sqrt{2\tau/T_t}$. An alternative viewpoint is that the time average $\langle \{Q\}_{N_{pc},M,\Delta t} \rangle_{T_t}$ is statistically equivalent to the ensemble average of $\langle Q \rangle$ over $I = R_Q^{-2}$ independent samples. For large T_t/τ, this number of sample is $I = T_t/(2\tau)$. Numerical experiment verifies Eq. (37) as well

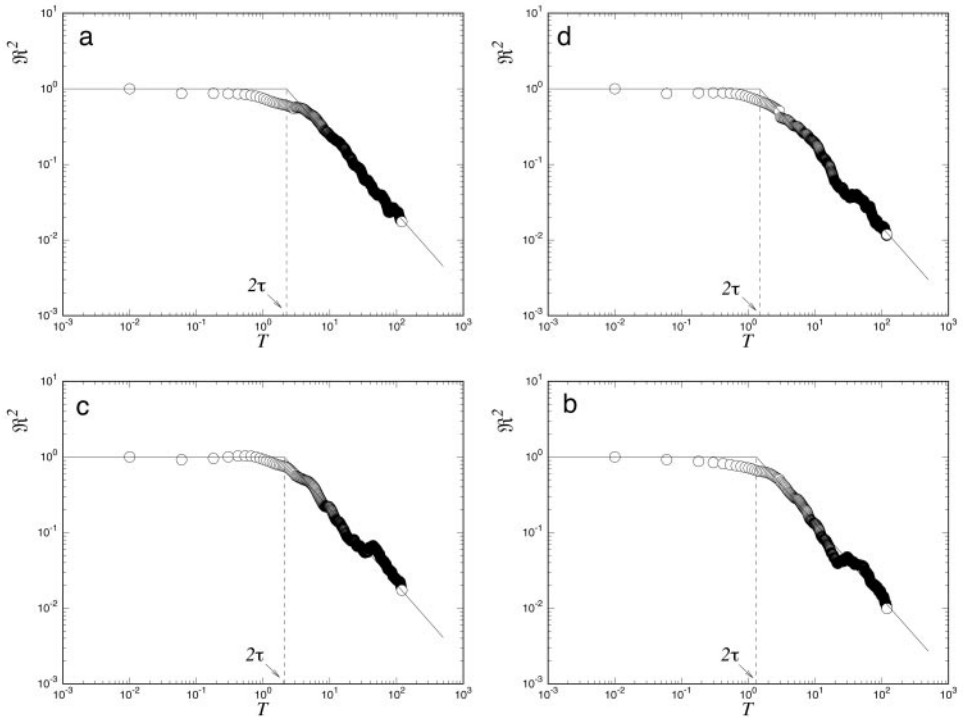

FIG. 6. Reduction factor of statistical error by time-averaging ($\mathcal{R}_Q$, Eq. (34)) and estimation of the time scale τ (Eq. (38)) for stationary solutions at point (40, 1.0). Line, estimation function ($\hat{\mathcal{R}}_Q$, Eq. (39)); symbols, estimate; (a) mean velocity; (b) turbulence energy; (c) mean frequency; (d) mean mixture fraction.

(Fig. 6). The advantage of time-averaging is obvious: for large T_t the statistical error can be reduced at will so that smoother results can be obtained. This is helpful to distinguish the deterministic error from the statistical error. Throughout the following discussion on bias and discretization error, the time-averaging is adopted to minimize the effect of the statistical error.

Obviously, the time scale τ essentially determines the efficiency of reducing the statistical error by the time-averaging technique. To estimate τ in the stationary time series of length T_t for a mean quantity, we can make use of the results of Eqs. (36), (37), and Fig. 6. The basic idea is to approximate Eq. (36) by an estimation function

$$\hat{\mathcal{R}}_Q^2(T) = \begin{cases} 1 & \text{for } T \le 2\tau, \\ 2\tau/T & \text{otherwise.} \end{cases} \tag{39}$$

Then a good estimate of τ is the value which minimizes the weighted mean square difference between $\mathcal{R}_Q$ and $\hat{\mathcal{R}}_Q$,

$$\chi(\tau) \equiv \int_0^\infty (\hat{\mathcal{R}}_Q(s) - \mathcal{R}_Q(s))^2 w(s)\, ds, \tag{40}$$

where the weight w is taken $w(s) = 1/s$. We performed 30 independent but identical simulations to obtain 30 independent stationary time series for estimated mean quantities. From these samples, τ is estimated using the above approach. As an example, the reduction factor

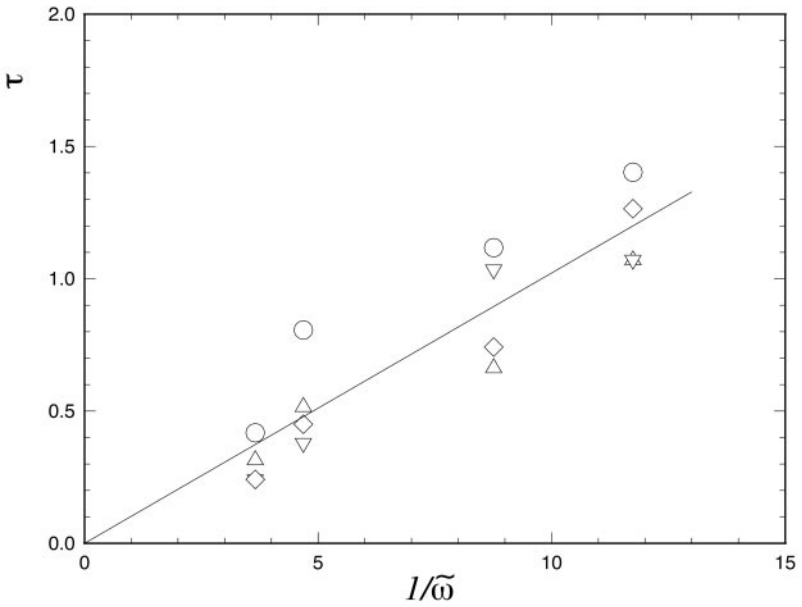

FIG. 7. Time scales τ of stationary mean fields. ○, mean velocity; △, turbulence energy; ▽, mean frequency; ◇, mean mixture fraction. (Locations, in order of increasing $\tilde{\omega}^{-1}$, (10, 0.5), (20, 1.0), (40, 1.0), (40, 2.5).)

against the time-averaging time scale is plotted in Fig. 6 for the observation point (40, 1.0). The estimated time scales τ for different locations are plotted in Fig. 7. It is implied that

$$\tau \simeq d/\tilde{\omega}, \tag{41}$$

where the constant d is about 0.1. That is, the time scale is about a tenth of the local time scale $\tilde{\omega}^{-1}$.

Statistical error can also be decreased by multiple independent simulations (MIS). *PDF2DV* is parallelized through particle partitioning and also can be used to make multiple independent simulations [37]. Suppose that we have a distributed-memory computer with $\mathcal{M}$ processors, and let each of them perform a statistically identical but independent simulation. At any time during the calculation, the mean fields and sample variance can be calculated over all particles that are gathered from all processors through the message passing method. For $\mathcal{M}$ independent samples of $\{Q\}^{(i)}_{N_{pc},M,\Delta t}$ $(i = 1, \ldots, \mathcal{M})$, an ensemble mean is formed

$$\left\langle \{Q\}_{N_{pc},M,\Delta t} \right\rangle_{\mathcal{M}} = \frac{1}{\mathcal{M}} \sum_{i=1}^{\mathcal{M}} \{Q\}^{(i)}_{N_{pc},M,\Delta t}. \tag{42}$$

It is easy to show that this approach reduces the statistical error by a factor of $\mathcal{M}^{-1/2}$. Also, the 95 percent confidence interval for the mean quantities can be estimated as

$$\delta_{CI} = 1.69 \left[\frac{1}{\mathcal{M}-1} \sum_{i=1}^{\mathcal{M}} \left(\{Q\}^{(i)}_{N_{pc},M,\Delta t} - \left\langle \{Q\}_{N_{pc},M,\Delta t} \right\rangle_{\mathcal{M}} \right)^2 \right]^{1/2}. \tag{43}$$

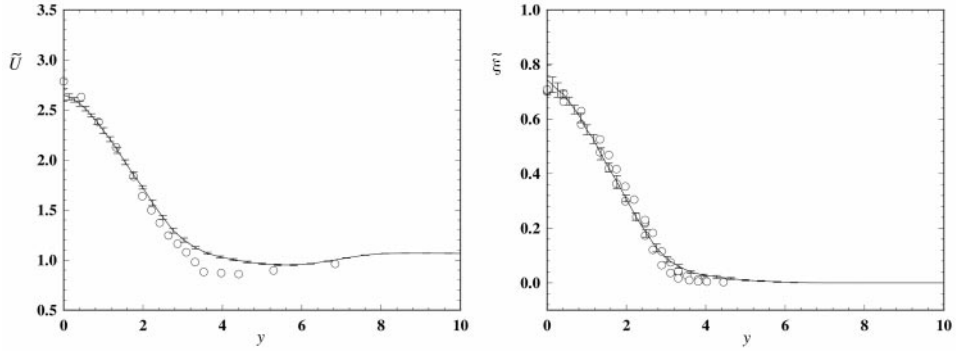

FIG. 8. Mean profiles from multiple independent simulations (MIS) at $x = 40$. Symbols are experimental data. Error bars indicate 95% confidence intervals. Cells, 40×40, $N_{pc} = 200$, and $\mathcal{M} = 10$.

Figure 8 gives the radial profiles of mean velocity and mixture fraction and their confidence intervals obtained with $\mathcal{M} = 10$ in comparison to experimental data. The statistical error reduction by MIS is effective.

5.3. *Bias*

Bias is the deterministic error caused by using a finite number of particles. Using the decomposition of numerical error in Subsection 3.2, the bias B_Q in the estimator $\{Q\}_{N_{pc},M,\Delta t}$ can be written

$$B_Q(N_{pc}, M, \Delta t) = \left\langle \{Q\}_{N_{pc},M,\Delta t} \right\rangle - \{Q\}_{\infty,M,\Delta t}. \tag{44}$$

The major source of bias is statistical errors in the coefficients of the SDEs. The features of bias have been studied by several authors for different PDF methods [40, 52, 55, 54]. Both analysis and numerical experiments have shown that the bias scales as Eq. (25) which is rewritten

$$B_Q = \frac{b_Q(M)}{N_{pc}}, \tag{45}$$

where the error coefficient b_Q indicates the size of bias given N_{pc}. Here, b_Q is explicitly expressed as a function of only M since it has been verified that B_Q is independent of Δt for stationary solutions [40, 52, 55].

Calculations are performed for different values of N_{pc}, but the same values of M and Δt to examine Eq. (45). Results are demonstrated by Fig. 9 where the time-averaged mean quantities are used to take the advantage of minimizing the influence of statistical error. A linear relationship between B_Q and N_{pc}^{-1} is very clear. Consequently, b_Q can be estimated through two calculations with $N_{pc} = N_{pc}^{(1)}$ and $N_{pc}^{(2)}$:

$$b_Q(M) = \frac{N_{pc}^{(1)} N_{pc}^{(2)}}{N_{pc}^{(2)} - N_{pc}^{(1)}} \left(\{Q\}_{N_{pc}^{(1)},M,\Delta t} - \{Q\}_{N_{pc}^{(2)},M,\Delta t} \right). \tag{46}$$

The slopes of straight lines in Fig. 9 correspond to b_Q.

With the frequency model based on the square of the mean rate of strain Eq. (5), Xu and Pope [55] discovered that b_Q exponentially increases as h decreases. This is a concern to

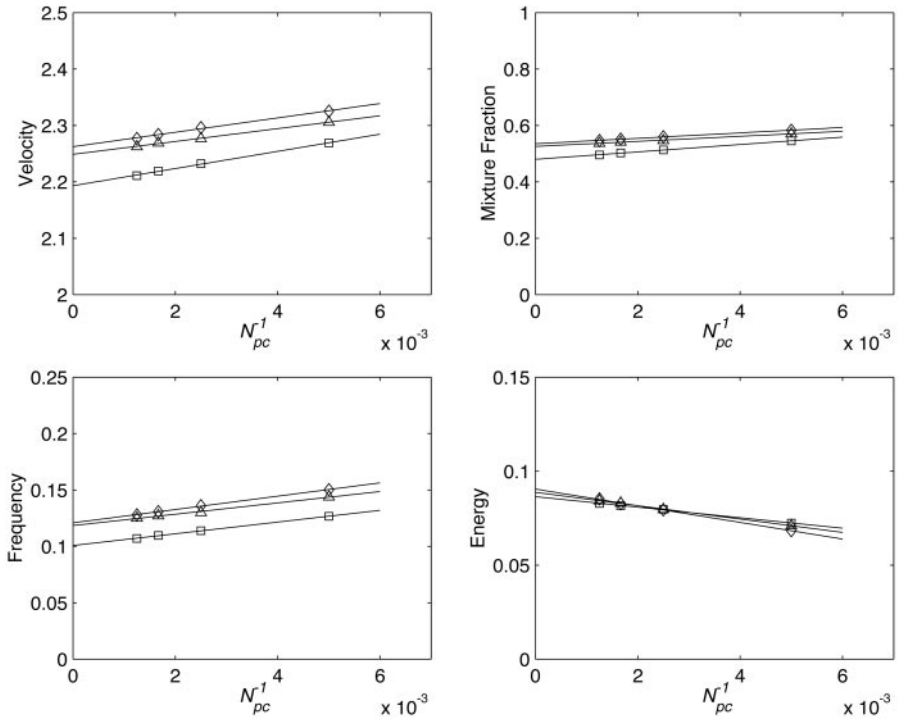

FIG. 9. Time-averaged mean quantities against N_{pc}^{-1} at (40, 1.0); lines are linear least-squares fits to the symbols. Cells, □, 30 × 30; △, 40 × 40; ◇, 50 × 50.

numerical convergence and computational cost since it means that a better spatial resolution is essentially penalized by a bigger bias. It also implies that more particles per cell are required for finer cells to maintain the accuracy, and this therefore dramatically increases the computational expense. In this study, the frequency model is modified such that the source is based on the production-to-dissipation ratio instead. For two representative observation points, the estimates of b_Q by Eq. (46) are plotted against cell size in Fig. 10. These results do not show the strong and consistent increase of bias with decreasing cell size observed in [55]. Instead, the majority of the data show that the bias varies little or decreases with decreasing cell size. The only exception is $|b_k|$ at the point (40, 1) which increases by 60% over the range of M considered.

5.4. *Discretization Error*

For the discretization error, neglecting the temporal error as discussed in Subsection 3.2, our focus is on the spatial error which is due to the finite size of cells. There has been no study of this error for the PDF particle-mesh method. The reason is that the spatial error can only be explored in the computation of inhomogeneous flows, and that the spatial error must be isolated from the bias and the statistical error. Thus it is a very expensive task to do so. The attempt is made here to explore the characteristics of spatial error.

The major source of the spatial error in *PDF2DV* is the estimation of mean fields by the cloud-in-cell method. In this method, a smaller value of h (or larger M) with N_{pc} unchanged yields a more local, and hence more accurate estimate. The discretization S_Q is identified

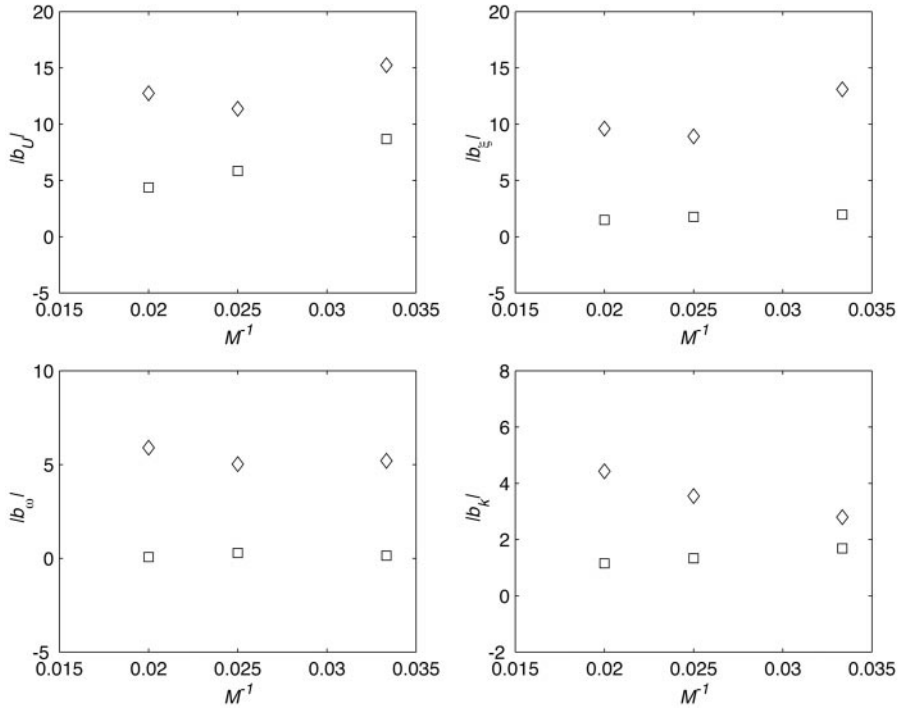

FIG. 10. Error coefficient b of bias against cells size, □, point (20, 2.5); ◇, point (40, 1.0).

as Eq. (26)

$$S_Q = \{Q\}_{\infty,M,\Delta t} - \langle Q \rangle. \tag{47}$$

The difficulty in estimating S_Q is to separate it from the bias B_Q. Since B_Q decreases as N_{pc}^{-1} while S_Q is independent of N_{pc}, theoretically one can distinguish them from each other by making a calculation with infinity N_{pc} which is unfortunately not practical. However, alternatively, this task can also be carried out by the Richardson extrapolation. As in Fig. 9, a set of calculations are first made for different N_{pc} for given h and Δt to get the time-averaged ensemble mean $\langle \{Q\}_{N_{pc},M,\Delta t} \rangle_T$. Then, an estimate of the mean quantity Q_e for N_{pc} approaching infinity can be obtained by a simple Richardson extrapolation in the limit of $N_{pc}^{-1} = 0$. That is, Q_e is calculated by

$$Q_e = \frac{\sum_{i=1}^{\mathcal{M}} \left\langle \{Q\}^{(i)}_{N_{pc},M,\Delta t} \right\rangle_T - b \sum_{i=1}^{\mathcal{M}} \left(N_{pc}^{(i)}\right)^{-1}}{\mathcal{M}}, \tag{48}$$

where $N_{pc}^{(i)}$ is the number of particles per cell and $\langle \{Q\}^{(i)}_{N_{pc},M,\Delta t} \rangle_T$ is the time-averaged mean in the ith calculation, and $\mathcal{M}$ is the number of calculations ($\mathcal{M} \geq 2$). As a result, Q_e is solely a function of cell size h (or M^{-1}) and can thus be used to measure the spatial discretization error.

Figure 11 plots Q_e (as well as the time-averaged mean quantities for different N_{pc}) against M^{-2}. The observation that a linear relationship exists between M^{-2} and Q_e in the region of finer cells is of significance since it implies that a second-order accuracy of spatial

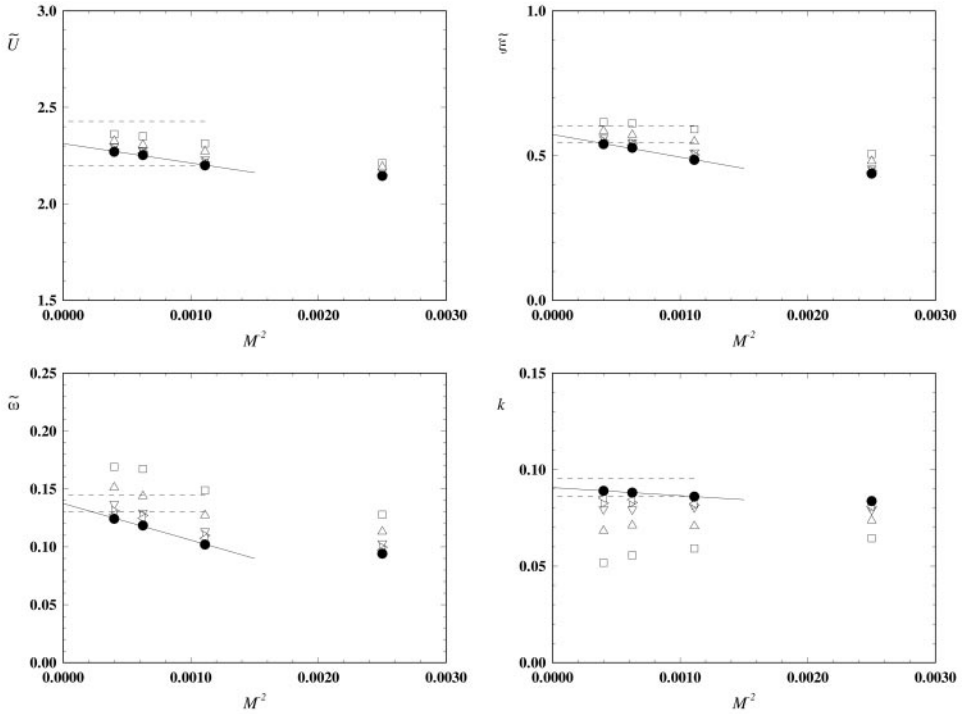

FIG. 11. Mean quantities against cell sizes at point (40, 1.0). Symbols, ●, Q_e (i.e., $N_{pc}=\infty$); □, $N_{pc}=100$; △, $N_{pc}=200$; ▽, $N_{pc}=400$; ▷, $N_{pc}=600$; ◁, $N_{pc}=800$. Solid lines are linear least-squares fits to Q_e for $M=30$, 40, and 50. Dashed lines indicate a ±5% error region of the estimates of mean quantities in the limit of $N_{pc}=\infty$ and $M=\infty$.

discretization error occurs in the particle-mesh method. Therefore, the discretization error can be written

$$S_Q = \frac{a_Q}{M^2}, \tag{49}$$

where a_Q is an error coefficient to be estimated.

Figure 11 also tells us how big the bias and spatial errors are. For example, to obtain a reasonable 5% accurate mean velocity, 40×40 cells and 100 particles per cell are enough at points $x=40$, $y=1.0$ and $x=40$, $y=2.5$ while it requires at least 50×50 and 400 particles per cell to get a 7% accuracy for turbulence energy. This is due to the effect of fluctuations in the first moments on the estimation of second moments.

The cell size dependence is also inspected in Fig. 12 in which time-averaged mean profiles are obtained for different grids. It is shown that the difference among profiles is decreasing with cell refinement.

Finally, one interesting observation is that for many cases, bias is partially cancelled out by the discretization error because of the opposite signs of a_Q and b_Q (Fig. 13). This is very encouraging since it can make the task of error reduction much easier, and therefore significantly reduces the computational cost, as seen later. However, it is to be addressed in future research why a_Q and b_Q have such a behavior.

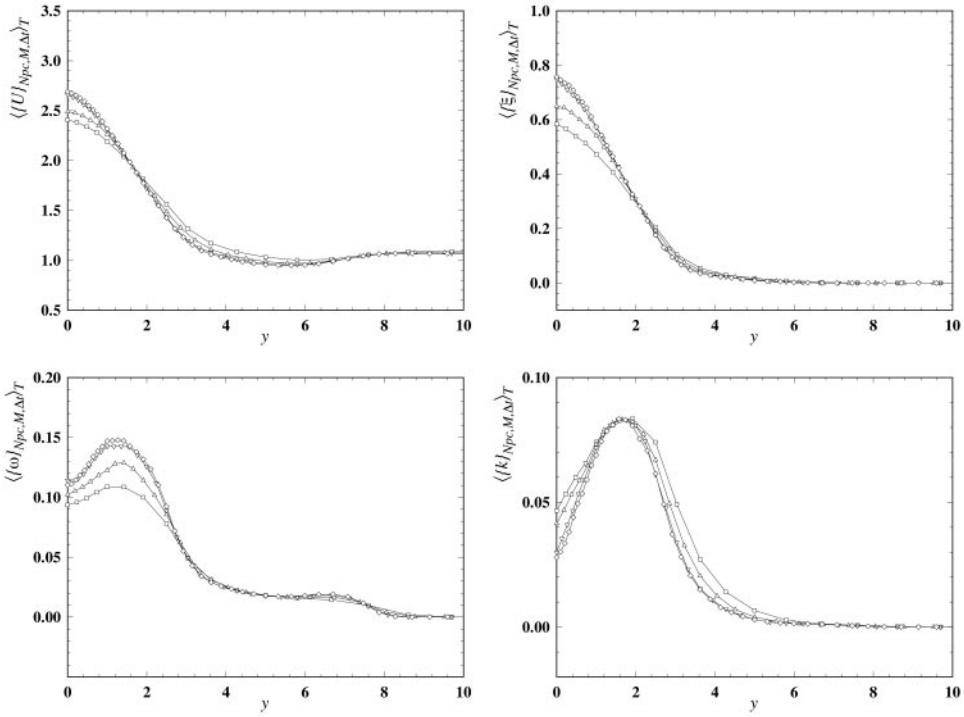

FIG. 12. Time-averaged mean profiles at $x = 40$ for different cells. □, 20×20; △, 30×30; ▽, 40×40; ◇, 50×50. $N_{pc} = 200$.

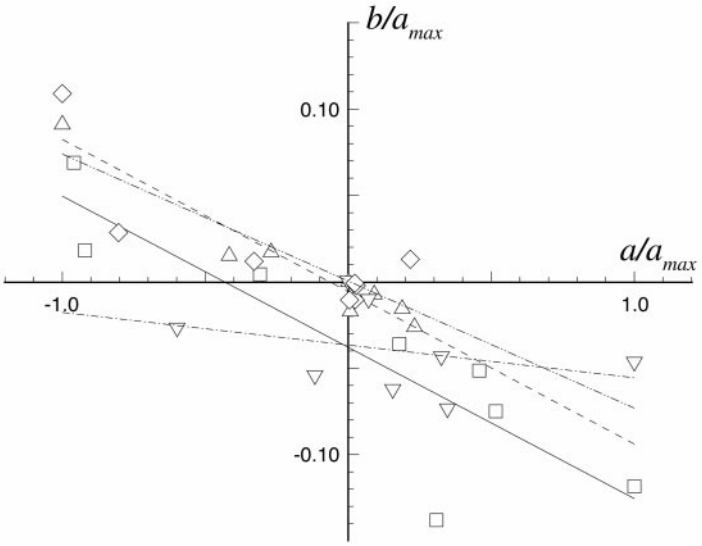

FIG. 13. Scatter plot of error coefficients a and b. Symbols, □, velocity; △, mixture fraction; ▽, turbulence energy; ◇, mixture fraction. Lines are linear least-squares fits to the symbols: solid, velocity; dashed, mixture fraction; dashed-dotted, turbulence energy; dash-dot-dotted, frequency.

5.5. *Summary*

The convergence study above leads to a plain and clear picture about the numerical errors in the particle-mesh method for PDF methods. The points that are worth emphasizing are

(1) All numerical errors have been quantified and characterized by N_{pc}, M, and I;
(2) Statistical error converges as $N_{pc}^{-1/2}$;
(3) Time-averaging and MIS can be used to reduce the statistical error;
(4) Bias scales as N_{pc}^{-1}, and thus converges faster than statistical error (but it is not removed by time-averaging or MIS);
(5) The modified model of frequency ameliorates dramatically the cell size dependence of bias revealed in previous study [55];
(6) With respect to the spatial discretization error, the method is second-order accurate, with S_Q converging at the rate of M^{-2}.

Putting Eqs. (33), (45), and (49) together, the total error in an estimator $\{Q\}_{N_{pc},M,\Delta t}$ becomes

$$\varepsilon_Q = S_Q + B_Q + \Sigma_Q = \frac{a_Q}{M^2} + \frac{b_Q}{N_{pc}} + \frac{c_Q}{\sqrt{I N_{pc}}}\vartheta, \tag{50}$$

where I equals $T_t/2\tau$ (for large T_t) representing the total number of independent samples in stationary solutions when time-averaging is used to reduce the statistical error, or $\mathcal{M}$ independent simulations when MIS is performed.

To conclude, in terms of numerical parameters of M and N_{pc}, the numerical solution of the particle-mesh algorithm is convergent. Therefore, *PDF2DV* can give as accurate results as desired by choosing appropriate M and N_{pc}. The next two sections attempt to estimate error coefficients a_Q, b_Q, and c_Q, error parameters such as I and the computational cost, and develop an effective error reduction scheme based on the above understandings of numerical errors.

6. ESTIMATION OF OPTIMAL NUMERICAL PARAMETERS

The quantification of numerical errors in terms of numerical parameters implies that one can make calculations of turbulent reactive flows using *PDF2DV* with specified accuracy by choosing a proper set of numerical parameters. The questions arising are

(1) What criterion for numerical accuracy should be chosen?
(2) What is the computational cost to achieve a certain level of accuracy?

Given a specified requirement of numerical accuracy, define the numerical parameters that minimize the computational cost subject to the specified accuracy as the *optimal parameters*. Then, the results from the forgoing section can be used to estimate the computational cost required to produce a calculation of specified accuracy, and the optimal parameters as functions of the specified level of accuracy. The estimation is done for the calculation of the piloted-jet flame using time-averaging. Therefore, the numerical parameters involved include the number of particles in each cell N_{pc}, the total number of cells M^2, and the number of independent samples I from a time series of mean quantities. The goal is to provide an insight of how to choose the optimal numerical parameters.

6.1. *Criterion for Numerical Accuracy*

This subsection is to address the first question above. Rewrite the total numerical error in terms of M, N_{pc}, and I

$$\varepsilon = S_Q + B_Q + \Sigma_Q = \frac{a}{M^2} + \frac{b}{N} + \frac{c}{\sqrt{I N_{pc}}}\vartheta. \tag{51}$$

Hereafter, the error (hence, a, b, and c) is normalized by the peak value of the local radial profile of mean fields. Also, for abbreviation, a_Q, b_Q, and c_Q have been replaced by a, b, and c, respectively.

Appreciating that the ϑ and hence ε are random variables, we therefore define $F(\delta)$ as the probability that the absolute total error is less than δ (positive number),

$$F(\delta) \equiv \text{Prob}\{|\varepsilon| \le \delta\}. \tag{52}$$

Hence, δ is the error tolerance. If ϑ is presumed to have a standardized Gaussian distribution, the above equations lead to

$$F(\delta) = \Phi\left(\frac{1-r}{s}\right) - \Phi\left(-\frac{1+r}{s}\right), \tag{53}$$

where

$$r = \frac{|S_Q + B_Q|}{\delta}, \qquad s = \frac{\sigma_Q}{\delta}, \tag{54}$$

and

$$\Phi(x) = \frac{1}{2}\left[1 + \text{erf}\left(\frac{x}{\sqrt{2}}\right)\right], \tag{55}$$

with erf representing the error function.

One criterion of acceptable accuracy, then, can be defined as that the probability $F(\delta)$ must be larger than a critical value F_c. For different F_c, the acceptable regions of r and s under this condition are shown in Fig. 14 under the contour lines $F(\delta) = F_c$.

Another criterion can be defined through a *weighted-error* ε_ν

$$\varepsilon_\nu \equiv |S_Q + B_Q| + \nu\sigma_Q, \tag{56}$$

where ν is a weight for the statistical error. Obviously, ε_ν is different from ε in that it is a deterministic error, and thus easier to handle. The criterion is defined by requiring that the weighted-error ε_ν is less than δ, i.e.,

$$\varepsilon_\nu = \delta(r + \nu s) \le \delta, \tag{57}$$

which leads to

$$r + \nu s \le 1. \tag{58}$$

The region under the dashed line in Fig. 14 corresponds to the acceptable region of Eq. (58) for $\nu = 1.3$.

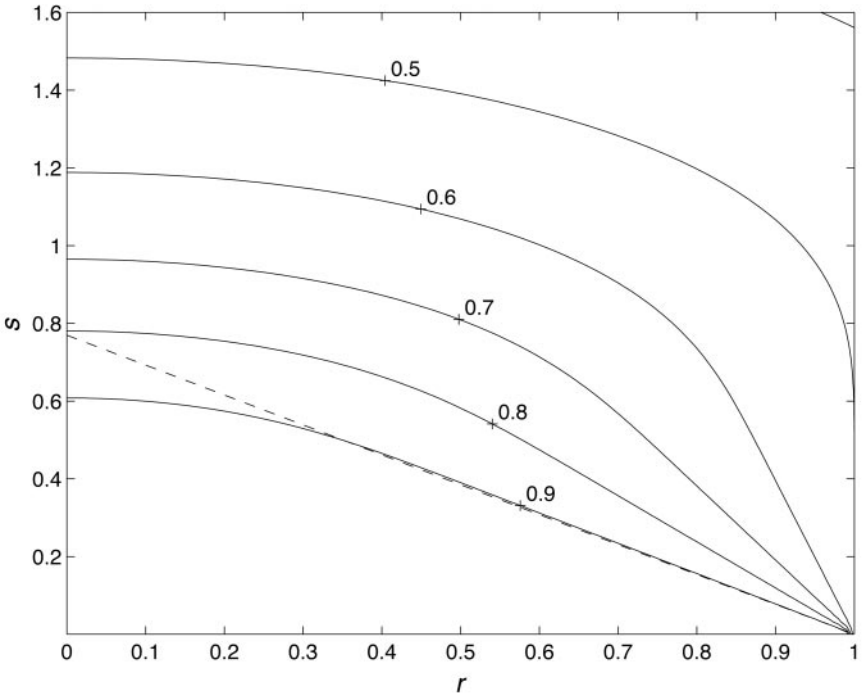

FIG. 14. Contour plot of $F(\delta)$ (Eq. (52), solid line) and ε_ν (Eq. (58) with $\nu = 1.3$, dashed line) as a function of s and r (Eq. (54)).

Hereafter, an accuracy of $\delta = 5\%$ in term of ε_ν is sought for the piloted-jet flame calculation. That is, Eq. (58) is to be satisfied. Figure 14 shows that the accept region of r and s satisfying Eq. (58) for $\nu = 1.3$ overlaps with the region satisfied by the first criterion with $F_c = 0.9$ except for a very small region, even in which $F(0.05)$ is bigger than 0.8. Therefore, it is reasonable to use second criterion with $\nu = 1.3$ and $\delta = 0.05$ with good agreement to the first criterion of $F_c = 0.9$.

We will consider a calculation in which time-averaging is used to reduce the statistical error. A consecutive stationary time series of length $T_t = N_t \Delta t$ is obtained after the solution reaches the stationary state in $T_s = N_s \Delta t$. As discussed above, this stationary time series contains $I = T_t/2\tau$ (for $T_t/\tau \gg 1$) independent samples, where τ is the underlying time scale of the time series. The total weighted-error becomes

$$\varepsilon_\nu = \frac{a}{M^2} + \frac{b}{N_{pc}} + \nu c \left(\frac{2\tau}{T_t N_{pc}} \right)^{1/2}. \tag{59}$$

This is the basic equation used in the next two sections.

6.2. *Estimation of Error Parameters*

Before we can use Eqs. (58) and (59), the error coefficients a, b, c, and other parameters, such as N_s and N_t, need to be estimated. Tables IV–VI list the estimated error coefficients a, b, and c, respectively, for eight different observation points. The maximum values are also given.

TABLE III
Time Steps against Cell Sizes

M	Δt	T_s	N_s	$\beta = N_s/M$
20	0.124	60	500	25
30	0.085	60	700	23
40	0.062	60	1000	25
50	0.050	60	1200	24

TABLE IV
Estimated Error Coefficients *a*

Points	$\tilde{U}$	$\tilde{\xi}$	k	$\tilde{\omega}$
(10, 0.5)	−38.4	−50.2	370.6	52.1
(20, 1.0)	−12.9	−32.6	128.5	−193.1
(20, 2.5)	19.1	22.7	120.6	5.7
(40, 1.0)	−40.0	−120.5	−43.3	−240.0
(40, 2.5)	41.7	27.9	57.6	−79.2
(40, 5.0)	21.5	10.9	26.2	6.7
(60, 5.0)	12.9	0.8	−221.8	1.0
(60, 10.0)	7.4	0.04	−0.58	5.4
max(|a|)	40.0	120.5	370.6	240.0

TABLE V
Estimated Error Coefficients *b*

Points	$\tilde{U}$	$\tilde{\xi}$	k	$\tilde{\omega}$
(10, 0.5)	0.76	1.82	−17.19	3.13
(20, 1.0)	0.18	2.06	−27.19	6.85
(20, 2.5)	−2.14	−1.88	−16.01	−2.49
(40, 1.0)	2.87	10.97	−20.07	26.20
(40, 2.5)	−4.94	−3.15	−23.04	2.86
(40, 5.0)	−3.12	−0.87	−3.72	−0.51
(60, 5.0)	−5.75	−2.07	−9.85	−2.53
(60, 10.0)	−1.50	−0.01	0.23	−0.20
max(|b|)	6.0	11.0	27.2	26.2

TABLE VI
Estimated Error Coefficients *c*

Points	$\tilde{U}$	$\tilde{\xi}$	k	$\tilde{\omega}$
(10, 0.5)	0.06	0.09	0.39	0.34
(20, 1.0)	0.09	0.23	0.91	0.49
(20, 2.5)	0.07	0.08	0.43	0.21
(40, 1.0)	0.10	0.34	0.83	0.46
(40, 2.5)	0.13	0.29	0.59	0.52
(40, 5.0)	0.05	0.05	0.08	0.09
(60, 5.0)	0.28	0.22	4.22	0.52
(60, 10.0)	0.06	0.0001	0.2l	0.07
max(|c|)	0.3	0.35	4.22	0.5

The other two parameters to be estimated for the purpose of estimating computational work are N_s, the time steps required from the initial state to the stationary state, and N_t, the time steps for time-averaging. The time step is well represented by

$$\Delta t \sim \frac{\mathcal{L}_x}{\tilde{U}M}. \tag{60}$$

Note that $\mathcal{L}_x$ and $\tilde{U}$ are non-dimensional scale and velocity normalized by R_j and U_C, respectively. Hence, Δt is also a non-dimensional time step. For a given flow, Eq. (60) implies that

$$\Delta t = (\kappa M)^{-1}, \tag{61}$$

where $\kappa = 0.4$ as shown in Fig. 15 and Table III for the piloted-jet flame. Then,

$$N_s \propto T_f/\Delta t \propto M, \tag{62}$$

where T_f is the flow residence time. Hence, it is reasonable to argue that

$$N_s = \beta M. \tag{63}$$

The estimation from the calculations gives $\beta \simeq 25$ (Table III).

On the other hand, if I independent samples from a time series of mean quantities are desired for a certain level of numerical accuracy, then

$$N_t = \frac{2I\tau}{\Delta t} = \mu M I, \tag{64}$$

where $\mu = 2\kappa\tau$. Since τ is related to the local time scale, μ varies in the domain. At this point, we are ready for estimating the computational work and optimal numerical parameters.

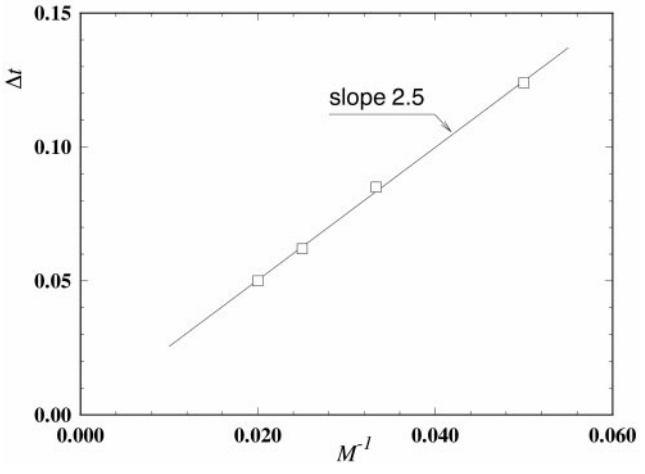

FIG. 15. Time step against characteristic cell size M^{-1}.

6.3. *Computational Work and Optimal Numerical Parameters*

The computational work in a PDF calculation with M^2 cells, N_{pc} particles per cell, and a total of $N_t = N_s + N_t$ time steps can be measured by

$$W \equiv M^2 N_{pc}(N_s + N_t). \tag{65}$$

If t_c denotes the average CPU time for a particle in each time step (approximately $t_c = 4.5 \times 10^{-5}$ s on an SGI Indigo 2 workstation), then Wt_c is the total CPU time for the full-scale calculation. Here, we use the piloted-jet flame problem as an example to demonstrate how to estimate the computational work and optimal numerical parameters. Substituting Eqs. (63) and (64) into Eq. (65) yields

$$W = M^3 N_{pc}(\beta + \mu I). \tag{66}$$

The interesting question addressed here is that what are the optimal numerical parameters that minimize W subject to the condition

$$\varepsilon_v = \left| \frac{a}{M^2} + \frac{b}{N_{pc}} \right| + \nu \frac{c}{\sqrt{I N_{pc}}} \leq \delta. \tag{67}$$

This is a constrained optimization problem, and there are three parameters to be determined: M, N_{pc}, and I.

To proceed with the analysis, we assume that a and b are of the same sign. Unfortunately, this leads to a grossly inaccurate estimate of the work required—too large by as much as a factor of 100. This is because it is found that a and b tend to have opposite signs (see Fig. 13). The assumption of the cancellation between a and b allows M and N_{pc} to be chosen so that the deterministic error vanishes. But in practice, a and b are not known a priori, nor are they the same at all locations and for all quantities. Hence, the estimates based on this assumption are grossly in error as well.

The Lagrangian multiplier method is used to solve such a constrained optimization problem. Let

$$\begin{aligned} G &\equiv W + \lambda(\varepsilon_v - \delta), \\ &= M^3 N_{pc}(\beta + \mu I) + \lambda\left(aM^{-2} + bN_{pc}^{-1} + \nu c I^{-1/2} N_{pc}^{-1/2} - \delta\right), \end{aligned} \tag{68}$$

where λ is the Lagrangian multiplier, and for convenience, we have implicitly assumed that a and b take their absolute values. Then, the optimal values of M, N, and I are solved from the following equations:

$$\frac{dG}{dM} = 3M^2 N_{pc}(\beta + \mu I) - 2\lambda a M^{-3} = 0, \tag{69}$$

$$\frac{dG}{dN_{pc}} = M^3(\beta + \mu I) - \lambda\left(bN_{pc}^{-2} + \frac{1}{2}\nu c I^{-1/2} N_{pc}^{-3/2}\right) = 0, \tag{70}$$

$$\frac{dG}{dI} = \mu M^3 N_{pc} - \frac{1}{2}\lambda \nu c I^{-3/2} N_{pc}^{-1/2} = 0, \tag{71}$$

$$\frac{dG}{d\lambda} = aM^{-2} + bN_{pc}^{-1} + \nu c I^{-1/2} N_{pc}^{-1/2} - \delta = 0. \tag{72}$$

These are a set of non-linear equations and can be solved through numerical solution [44].

TABLE VII
Estimated Computational Work and Optimal Numerical Parameters Subject to 5% Error at Point (40, 1.0)

Parameters	$\tilde{U}$	$\tilde{\xi}$	k	$\tilde{\omega}$
a	40.00	120.50	43.30	240.00
b	2.87	10.97	20.07	26.20
c	0.10	0.34	0.83	0.46
M	37	65	40	92
N_{pc}	169	692	1406	1621
I	5.44	8.05	12.36	7.32
N_s	933	1633	991	2300
N_t	118	305	284	391
W	2.5×10^8	5.7×10^9	2.8×10^9	3.7×10^{10}
CPU	3.09	71.58	35.24	461.60
S_Q	0.029	0.028	0.028	0.028
B_Q	0.017	0.016	0.014	0.016
Σ_Q	0.003	0.005	0.006	0.004

Note. CPU times correspond to the number of hours on SGI workstation (MIPS R8000 Processor plus R8010 Floating Point Chip). The error coefficients are assigned their absolute values.

We estimate the optimal computational work and numerical parameters using the error coefficients at point (40, 1.0). According to Tables IV–V, this is the worst case in terms of error size, particularly in the mean mixture fraction. The results are listed in Table VII for the case of using the absolute values of a and b. The estimated computational cost is obviously too large with respect to the mean frequency. However, if the real values of a and b are used instead to do the estimation, the CPU time is dramatically dropped since a and b cancel out with each other. This is seen in Table VIII.

TABLE VIII
Estimated Computational Work and Optimal Numerical Parameters Subject to 5% Error at Point (40, 1.0)

Parameters	$\tilde{U}$	$\tilde{\xi}$	k	$\tilde{\omega}$
a	−40.00	−120.50	−43.30	−240.00
b	2.87	10.97	−20.07	26.20
c	0.10	0.34	0.83	0.46
M	30	30	40	30.00
N_{pc}	35	70	1406	93.60
I	3.22	3.75	12.36	2.83
N_s	750	750	991	750
N_t	56	65	284	49
W	2.5×10^7	5.1×10^7	2.8×10^9	6.7×10^7
CPU	0.32	0.64	35.24	0.84
S_Q	−0.044	−0.134	−0.028	−0.267
B_Q	0.082	0.157	−0.014	0.280
Σ_Q	0.009	0.021	0.006	0.028

Note. CPU times correspond to the number of hours on SGI workstation (MIPS R8000 Processor plus R8010 Floating Point Chip). The error coefficients are assigned their actual values.

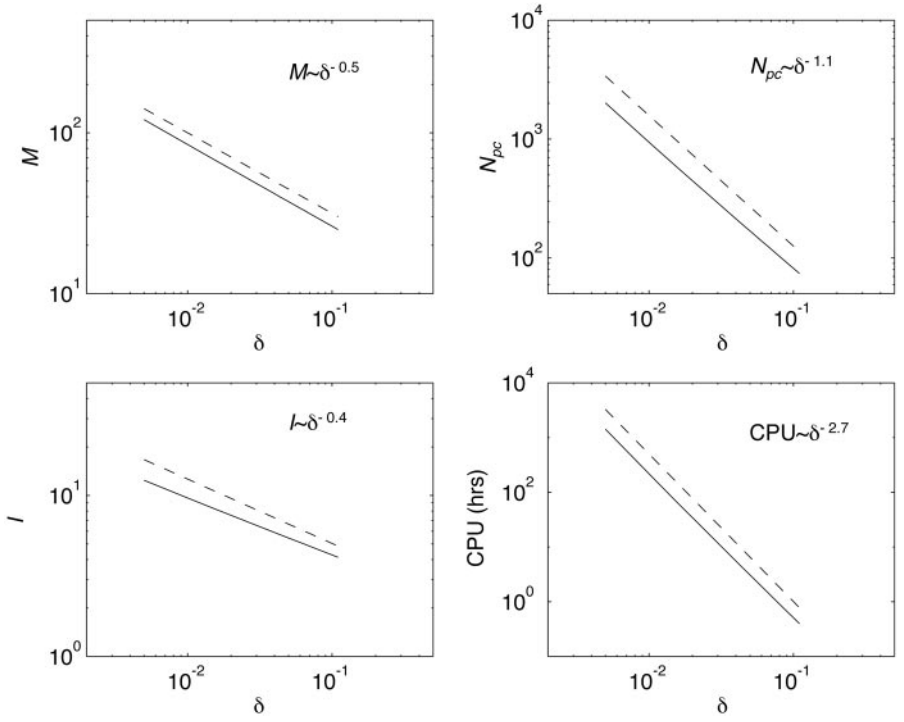

FIG. 16. Estimated optimal parameters against error tolerance obtained from Eqs. (69)–(72) using error coefficients associated with mean velocity at (40, 1.0). The dashed lines are power laws shown for comparison.

We have seen that the analysis with the assumption that a and b are of the same sign overestimates the work requirement by as much as a factor of 100. Nevertheless, we continue to explore the dependence of the optimal parameters (given by the analysis) as functions of the error tolerance δ. Figure 16 gives an impression of how the optimal computational work increases when the error tolerance δ decreases: M at the rate of $\delta^{-0.5}$; $N_{pc} \sim \delta^{-1.0}$; $I \sim \delta^{-0.4}$; and CPU $\sim \delta^{-3.0}$. The optimized errors are plotted against the error tolerance δ in Fig. 17. It shows that the spatial error is the major contribution, while the statistical error is relatively small, in particular when δ is larger. This explains why I is relatively small (Table VII).

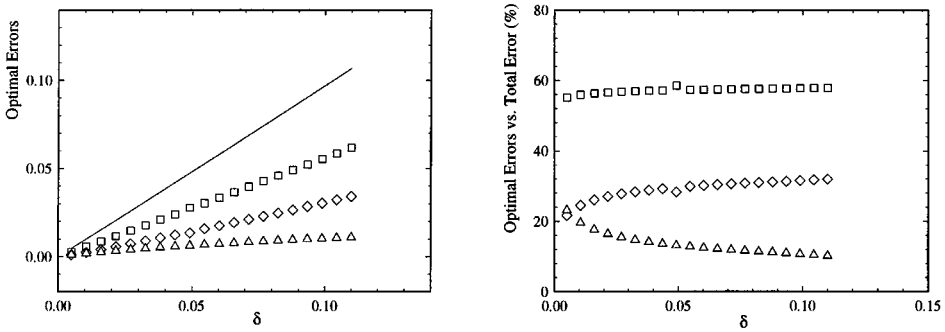

FIG. 17. Estimated optimal errors against error tolerance obtained from Eqs. (69)–(72) using error coefficients associated with mean velocity at (40, 1.0). Solid line, the total error; □, spatial error; ◇, bias; △, statistical error.

However, it should be noticed that the above analysis is based on the assumption that I is much larger than unity.

7. AN ERROR REDUCTION SCHEME

The objective of this section is to develop an error reduction scheme for the deterministic error—the sum of the bias and the spatial error, such that the computational work is also reduced. The deterministic error to leading order in the estimate of $\langle Q \rangle$ is

$$D_Q \equiv S_Q + B_Q = \frac{a}{M^2} + \frac{b}{N_{pc}}. \tag{73}$$

The second equality is true as M is large enough, say $M \geq 30$ in the piloted-jet flame as discovered in Section 5. The analysis and scheme presented here are based on the assumption that the coefficient of bias b is independent of M. This is a reasonable assumption given the observed behavior of the bias (see Fig. 10), but it is recognized not to be uniformly accurate.

Suppose that two calculations with different sets of numerical parameters (M_1, N_1) and (M_2, N_2) are performed and make these parameters satisfy

$$\alpha \equiv \frac{M_2}{M_1} = \sqrt{\frac{N_2}{N_1}} > 1. \tag{74}$$

The corresponding estimates of $\langle Q \rangle$ are denoted as

$$Q_1 = Q_{N_1, M_1}, \qquad Q_2 = Q_{N_2, M_2}, \tag{75}$$

where the time step effect has been implicitly neglected as suggested in Sections 3 and 5. The results from the previous sections suggest that

$$Q_1 = \langle Q \rangle + D_{Q_1} + \Sigma_{Q_1} = \langle Q \rangle + \frac{a}{M_1^2} + \frac{b}{N_1} + \frac{c\vartheta_1}{(I_1 N_1)^{1/2}}, \tag{76}$$

and

$$Q_2 = \langle Q \rangle + D_{Q_2} + \Sigma_{Q_2} = \langle Q \rangle + \frac{a}{M_2^2} + \frac{b}{N_2} + \frac{c\vartheta_2}{(I_2 N_2)^{1/2}}, \tag{77}$$

where I_1 and I_2 are the number of independent samples in the time series of mean fields from the two calculations, respectively. Note that a and b are the same for the two calculations, and ϑ_1 and ϑ_2 are independent standardized random variables. Also, because of the condition Eq. (74), it is true that

$$D_{Q_2} = \frac{D_{Q_1}}{\alpha^2}. \tag{78}$$

Now, we use Richardson extrapolation to define a new estimate for $\langle Q \rangle$

$$Q_r \equiv \frac{\alpha^2 Q_2 - Q_1}{\alpha^2 - 1}. \tag{79}$$

The error in Q_r can be decomposed into deterministic error and statistical error

$$Q_r = \langle Q \rangle + D_{Q_r} + \Sigma_{Q_r}. \tag{80}$$

It is an easy task to evaluate D_{Q_r}, i.e.,

$$D_{Q_r} = \frac{\alpha^2 D_{Q_2} - D_{Q_1}}{\alpha^2 - 1} = 0. \tag{81}$$

The deterministic error in Q_r vanishes. In this sense, Q_r is undoubtedly a better estimate for $\langle Q \rangle$ than Q_1 and Q_2. However, it should be appreciated that the deterministic error D_Q is $a/M^2 + b/N_{pc}$ *to leading order*. It is this leading order error that cancels in Q_r, to leave smaller secondary errors.

However, it is readily shown that

$$\mathrm{var}(Q_r) = \frac{\alpha^2 \,\mathrm{var}(Q_2) + \mathrm{var}(Q_1)}{(\alpha^2 - 1)^2} = \frac{\alpha^2}{(\alpha^2 - 1)^2}\left(\alpha^2 + \frac{I_2}{I_1}\right)\frac{c^2}{N_2 I_2}. \tag{82}$$

Hence, the statistical error Q_r may be amplified. For example, with $I_1 = I_2$ and $\alpha^2 = 2$, $\mathrm{var}(Q_r) = 6c^2/N_2 I_2 = 6\,\mathrm{var}(Q_2)$: the rms statistical error is larger in Q_r than in Q_2 by a factor of $\sqrt{6}$. But it is cheaper to increase I by a factor of six than to decrease the deterministic error by other means.

This error reduction scheme is tested using different conditions of M and N. The test cases are listed in Table IX where for some cases Eq. (74) is not exactly satisfied and therefore both α_1 based on M and α_2 based on N (defined in the table) are tried. In Fig. 18, the relative total errors in Q_1, Q_2, and Q_r are illustrated for these cases (cases A–E). Note that the relative errors are calculated based on the "theoretical" model results which are the intersections at y axes in Fig. 11 in this case. In all the cases a total error less than 5% in Q_r is obtained. It shows that the error reduction scheme is very effective, especially when the errors are relatively large (e.g., for in the turbulence energy): the reduction scheme can effectively reduce the errors since it theoretically eliminates the deterministic error.

This scheme can also save a significant amount of computational time. As discussed in the previous section, to yield an error under 5% for turbulence energy, for the worst case the optimal values for M and N_{pc} are about 40 and 1400, respectively, which requires about 35 hours on the SGI Indigo 2 workstation (Table VIII). But using Richardson extrapolation, smaller error can be achieved with two cases $M = 30$, $N = 200$ and $M = 40$, $N = 350$ which together need about 15 hours.

TABLE IX
List of Cases Used to Examine Error Reduction Scheme

Case	Condition 1	Condition 2	α_1	α_2
A	$N_1 = 400$, $M_1 = 40$	$N_2 = 600$, $M_2 = 50$	~1.25	~1.22
B	$N_1 = 200$, $M_1 = 30$	$N_2 = 600$, $M_2 = 50$	~1.67	~1.73
C	$N_1 = 200$, $M_1 = 30$	$N_2 = 400$, $M_2 = 40$	~1.33	~1.41
D	$N_1 = 200$, $M_1 = 20$	$N_2 = 800$, $M_2 = 40$	2	2
E	$N_1 = 100$, $M_1 = 20$	$N_2 = 400$, $M_2 = 40$	2	2

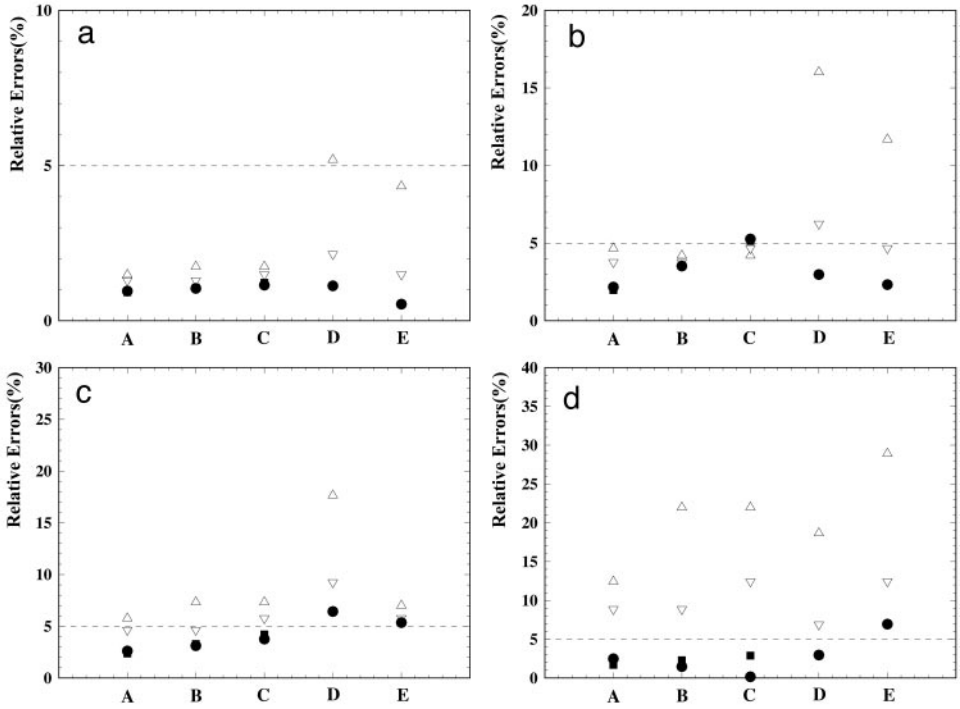

FIG. 18. Relative errors of mean quantities at point (40, 1.0) for the calculations given in Table IX. △, condition 1; ▽, condition 2; ●, extrapolating using α_1; boxes, extrapolating using α_2. Dashed lines shows 5% error. (a) Mean velocity; (b) mean mixture fraction; (c) mean frequency; (d) turbulence energy.

Finally, to make the use of this reduction scheme, we should emphasize that

(1) The numerical parameters should be chosen in such a way that, not only is Eq. (74) assured, but also M must be large enough to ensure second-order accuracy of the spatial error.

(2) Generally, the total error does not vanish since the statistical error cannot be eliminated by this scheme, but it does not have a substantial impact on the reduction of the deterministic error and the computational expense.

(3) The scheme is based on the assumption that the bias is independent of cell size. However, the results show that even if this assumption is not uniformly accurate, the algorithm is still effective in reducing the deterministic error.

(4) It is noted that the extrapolation technique requires the performance of two or three separate calculations. This is of course less convenient than performing a single calculation. But, in practice, this inconvenience is reduced by appropriate post-processing procedures, and the computational saving provided by the extrapolation scheme is worthwhile.

8. CONCLUSIONS

Accurate predictions of turbulent reactive flows need not only physically rational turbulence models, but also accurate numerical algorithms. This study investigates the numerical behaviors of PDF/Monte Carlo methods for turbulent reactive flows.

The joint velocity-frequency-composition PDF model is solved through a Monte Carlo method—particle-mesh approach. In this algorithm, the flow is modelled as an ensemble of stochastic particles. Particle properties evolve according to a set of stochastic differential equations that exhibit the same joint PDF as the modelled joint PDF transport equation. A pseudo-time marching scheme of second-order accuracy is used to solve the stochastic differential equations numerically. The flow field is also described by mean fields which are estimated through kernel estimation (cloud-in-cell method) by dividing the computational domain into a number of small cells. This particle-mesh algorithm is currently implemented in the *PDF2DV* code which has been adopted in several published applications of 2-D or axi-symmetric flows.

A modified model based on turbulence production-to-dissipation ratio is suggested for turbulence frequency in order to improve the numerical performance of the joint velocity-frequency-composition PDF model. The purpose is to remedy the problem found in a previous study that one of the numerical errors—bias—increases when the cell size is reduced.

Numerical experiments are conducted systematically and comprehensively on a test case—the piloted-jet nonpremixed turbulent flame of methane. To obtain numerical solutions in good agreement with experimental data, it is realized that the boundary conditions require careful specification for the modified turbulence frequency model. After a reasonable comparison is achieved, the focus of this study is then on the convergence of *PDF2DV* through characterizing various numerical errors.

The numerical errors are first decomposed into statistical error, bias, and discretization error. Both the statistical error and the bias arise due to the finite number of particles while the finite value of cell size and time step leads to the discretization error. The stationarity of numerical solutions is examined and verified to be independent of time step Δt. The numerical errors are investigated individually through varying numerical parameters: the number of particles in each cell N_{pc} and the total number of cells M^2. It is revealed that the statistical error converges as $N_{pc}^{-1/2}$, the bias scales as N_{pc}^{-1}, and that the use of the modified frequency model based on the production-to-dissipation ratio can dramatically ameliorate the cell size dependence of bias. Numerical experiments are also performed to understand the spatial discretization error for the first time. Second-order accuracy with respect to the spatial discretization is demonstrated. To summarize, the particle-mesh method in *PDF2DV* is convergent in terms of numerical parameters, N_{pc}, M^2, and Δt, and therefore one can obtain as accurate results as required by choosing the parameters correspondingly.

The quantification of numerical errors in terms of N_{pc} and M also provides the opportunity of estimating the computational requirement for an accurate calculation. The optimal numerical parameters minimizing the computational work subject to a specified level of error tolerance are evaluated. It is found that there exists a cancellation between the bias and the discretization error. This fact dramatically reduces the computational work, however, future work needs to be done to understand this phenomenon and to assess its generality. The results show that to achieve a reasonable 5% relative error (total error), the CPU time on an SGI Indigo 2 workstation required is less than 1 hour for the mean velocity, but about 35 hours for the turbulence kinetic energy.

The time-averaging technique is an useful approach to reduce statistical error. The reduction of statistical error can also be accomplished by multiple independent simulations with the parallelized program.

An effective error reduction scheme is proposed based on Richardson extrapolation to reduce the deterministic error. The scheme is shown to be capable of reducing the leading error, i.e., the sum of bias and discretization, by using two calculations with properly prescribed numerical parameters.

ACKNOWLEDGMENTS

This work was supported by Air Force Office of Scientific Research Grant F49620-97-1-0126. We are grateful to Dr. N. Peters and his research group for providing us with the flamelet libraries for methane combustion. Some computations were performed on the Cornell Theory Center's supercomputer, which is supported in part by the National Science Foundation, New York State, and the IBM Corporation. The authors also thank the reviewers for their valuable suggestions on improving the paper.

REFERENCES

1. M. S. Anand, A. T. Hsu, and S. B. Pope, Calculations of swirl combustors using joint velocity-scalar probability density function method, *AIAA J.* **35**(6), 1143 (1997).
2. R. S. Barlow (Ed.), *First International Workshop on Measurement and Computation of Turbulent Nonpremixed Flames* (Naples, Italy, 1996).
3. G.-C. Chang, *A Monte Carlo PDF/Finite-Volume Study of Turbulent Flames*, Ph.D. thesis, Cornell University, 1996.
4. J. Y. Chen, W. Kollmann, and R. W. Dibble, PDF modelling of turbulent nonpremixed methane jet flames, *Combust. Sci. Technol.* **64**, 315 (1989).
5. S. M. Correa and S. B. Pope, Comparison of a Monte Carlo PDF finite-volume mean flow model with bluff-body Raman data, in *Twenty-Fourth Symp. (International) on Combust.* (The Combustion Institute, Pittsburgh, 1992), p. 279.
6. B. Delarue and S. B. Pope, Application of PDF methods to compressible turbulent flows, *Phys. Fluids* **9**(9), 2704 (1997).
7. C. Dopazo, Probability density function approach for a turbulent axisymmetric heated jet: Centerline evolution, *Phys. Fluids A* **18**(2), 389 (1975).
8. C. Dopazo, Recent developments in pdf methods, in *Turbulent Reacting Flows*, edited by P. A. Libby and F. A. Williams (Academic Press, San Diego, 1994), p. 375.
9. T. D. Dreeben and S. B. Pope, *Nonparametric Estimation of Mean Fields with Application to Particle Methods for Turbulent Flows*, Technical Report FDA 92-13, Cornell University, 1992.
10. T. D. Dreeben and S. B. Pope, Probability density function Monte Carlo simulation of near-wall turbulent flows, *J. Fluid Mech.* **357**, 141 (1998).
11. K. Hanjalić and N. Stŏsić, Hysteresis of turbulent stresses in wall flows subjected to periodic disturbances, in *Turbulent Shear Flows* (Springer-Verlag, 1983), Vol. 4.
12. W. Härdle, *Applied Nonparametric Regression* (Cambridge Univ. Press, Cambridge, 1989).
13. D. C. Haworth and S. B. Pope, A generalized Langevin model for turbulent flows, *Phys. Fluids* **29**(2), 387 (1986).
14. D. C. Haworth and S. B. Pope, A second-order Monte Carlo method for the solution of the Ito stochastic differential equation, *Stochastic Anal. Appl.* **4**, 151 (1986).
15. D. C. Haworth and S. B. Pope, A pdf modeling study of self-similar turbulent free shear flows, *Phys. Fluids* **30**(4), 1026 (1987).
16. T. Hulek and R. P. Lindstedt, Joint scalar-velocity pdf modelling of finite rate chemistry in a scalar mixing layer, *Combust. Sci. Technol.* **136**, 303 (1998).
17. W. P. Jones, Turbulence modelling and numerical solution methods for variable density and combusting flows, in *Turbulent Reacting Flows*, edited by P. A. Libby and F. A. Williams (Academic Press, San Diego, 1994), p. 309.

18. W. P. Jones and M. Kakhi, Pdf modelling of finite-rate chemistry effects in turbulent nonpremixed jet flames, *Combust. Flame* **115**, 210 (1998).
19. M. H. Kalos and P. A. Whitlock, *Monte Carlo Methods* (Wiley, New York, 1986).
20. M. Kendall, A. Stuart, and J. K. Ord, *The Advanced Theory of Statistics*, 4th ed. (Griffin & Company Limited, England, 1983), Vol. 3.
21. Y. Komori and Y. Saito, Some issues in discrete approximate solution for stochastic differential equations, *Comput. Math. Appl.* **28**, 269 (1994).
22. R. J. Larsen and M. L. Marx, *An Introduction to Mathematical Statistics and Its Application*, 2nd ed. (Prentice Hall, International, Englewood Cliffs, NJ, 1986).
23. B. E. Launder, Phenomenological modelling: Present and future? in *Whither Turbulence? Turbulence at the Crossroads*, edited by J. L. Lumley (Springer-Verlag, New York, 1989).
24. B. E. Launder and D. B. Spalding, *Mathematical Models of Turbulence* (Academic Press, London, 1972).
25. S. Lee, The convergence of complex Langevin simulations, *Nuclear Phys. B* **413**, 827 (1994).
26. P. E. Kloeden and E. Platen, *Numerical Solution of Stochastic Differential Equations* (Springer-Verlag, New York/Berlin, 1992).
27. A. R. Masri and R. W. Bilger, Turbulent nonpremixed flames of hydrocarbon fuels near extinction: Mean structure from probe measurements, in *Twenty-First Symp. (International) on Combust.* (The Combustion Institute, Pittsburgh, 1988), p. 1511.
28. A. R. Masri, R. W. Dibble, and R. S. Barlow, The structure of turbulent nonpremixed flames revealed by Raman-Rayleigh-LIF measurements, *Prog. Energy Combust. Sci.* **22**(4), 307 (1996).
29. A. R. Masri and S. B. Pope, PDF calculations of piloted turbulent nonpremixed flames of methane, *Combust. Flame* **81**, 13 (1990).
30. J. P. Minier and J. Pozorski, Analysis of a PDF model in a mixing layer case, in *Tenth Symp. on Turb. Shear Flows, 1995*, p. 26:25.
31. T. V. Nguyen and S. B. Pope, Monte Carlo calculations of turbulent diffusion flames, *Combust. Sci. Technol.* **42**, 13 (1984).
32. P. A. Nooren, H. A. Wouters, T. W. J. Peeters, D. Roekaerts, U. Maas, and D. Schmidt, Monte Carlo PDF simulation of a turbulent natural-gas diffusion flame, in *Twenty-Sixth Symp. (International) on Combust* (The Combustion Institute, 1996).
33. A. T. Norris and S. B. Pope, Application of PDF methods to piloted diffusion flames: Sensitivity to model parameters, in *Eighth Symp. on Turb. Shear Flows* (Technical University of Munich, 1993).
34. N. Peters, personal communication.
35. S. B. Pope, A Monte Carlo method for the pdf equations of turbulent reactive flow, *Combust. Sci. Technol.* **25**, 159 (1981).
36. S. B. Pope, PDF methods for turbulent reactive flows, *Prog. Energy Combust. Sci.* **11**, 119 (1985).
37. S. B. Pope, PDF/Monte Carlo methods for turbulent combustion and their implementation on parallel computers, in *Turbulence and Molecular Processes in Combustion: A Collection of Contributions Based on Lectures Presented at the Sixth Toyota Conference* (Elsevier, New York, 1993).
38. S. B. Pope, Lagrangian PDF methods for turbulent flows, *Ann. Rev. Fluid Mech.* **26**, 23 (1994).
39. S. B. Pope, On the relationship between stochastic Lagrangian models of turbulence and second-moment closures, *Phys. Fluids* **6**(2), 973 (1994).
40. S. B. Pope, Particle method for turbulent flows: Integration of stochastic differential equations, *J. Comput. Phys.* **117**, 332 (1995).
41. S. B. Pope, *Position, Velocity and Pressure Correction Algorithm for Particle Method Solution of the pdf Transport Equations*, Technical Report FDA 95-06, Cornell University, 1995.
42. S. B. Pope, Computationally efficient implementation of combustion chemistry using *in situ* adaptive tabulation, *Combust. Theo. Modelling* **1**, 41 (1997).
43. S. B. Pope and Y. L. Chen, The velocity-dissipation probability density function model for turbulent flows, *Phys. Fluids A* **2**(8), 1437 (1990).
44. W. H. Press, S. A. Teukolsky, W. T. Vetterling, and B. P. Flannery, *Numerical Recipes in FORTRAN*, 2nd ed. (Cambridge Univ. Press, Cambridge, UK, 1992).

45. M. B. Priestley, *Spectral Analysis and Time Series* (Academic Press, San Diego, 1981).
46. V. Saxena and S. B. Pope, PDF calculations of major and minor species in a turbulent piloted-jet flame, in *Twenty-Seventh Symp. (International) on Combust.* (The Combustion Institute, Pittsburgh, 1998).
47. K. Seshadri and F. A. Williams, Reduced chemical systems and their application in turbulent combustion, in *Turbulent Reacting Flows*, edited by P. A. Libby and F. A. Williams (Academic Press, San Diego, 1994).
48. S. Subramaniam, *PDF Models for Mixing in Turbulent Reactive Flows*, Ph.D. thesis, Cornell University, 1997.
49. H. Tennekes and J. L. Lumley, *A First Course in Turbulence* (MIT Press, Cambridge, MA, 1972).
50. P. R. Van Slooten, Jayesh, and S. B. Pope, Advances in PDF modeling for inhomogeneous turbulent flows, *Phys. Fluid* **10**(1), 246 (1998).
51. M. P. Wand and M. C. Jones, *Kernel Smoothing* (Chapman & Hall, London, 1995).
52. W. C. Welton and S. B. Pope, PDF model calculations of compressible turbulent flows using smoothed particle hydrodynamics, *J. Comput. Phys.* **9**(4), 1085 (1997).
53. D. C. Wilcox, *Turbulence Modeling for CFD* (DCW Industries, Inc., La Cañada, CA, 1993).
54. J. Xu and S. B. Pope, *Analysis of Numerical Errors in Solving Particle Langevin Equations*, Technical Report FDA 97-07, Cornell University, 1997.
55. J. Xu and S. B. Pope, *Sources of Bias in Particle-Mesh Methods for PDF Models for Turbulent Flows*, Technical Report FDA 97-01, Cornell University, 1997.